SANDIA REPORT

SAND2014-1459
Unlimited Release
Printed February 2014

Geomechanical Testing of Bayou Choctaw 102B Core for SPR Analysis

Mathew D. Ingraham, Scott T. Broome, Stephen J. Bauer, Perry C. Barrow and Gregory M. Flint

Prepared by
Sandia National Laboratories
Albuquerque, New Mexico 87185 and Livermore, California 94550

Sandia National Laboratories is a multi-program laboratory managed and operated by Sandia Corporation, a wholly owned subsidiary of Lockheed Martin Corporation, for the U.S. Department of Energy's National Nuclear Security Administration under contract DE-AC04-94AL85000.

Approved for public release; further dissemination unlimited.

Sandia National Laboratories

Issued by Sandia National Laboratories, operated for the United States Department of Energy by Sandia Corporation.

NOTICE: This report was prepared as an account of work sponsored by an agency of the United States Government. Neither the United States Government, nor any agency thereof, nor any of their employees, nor any of their contractors, subcontractors, or their employees, make any warranty, express or implied, or assume any legal liability or responsibility for the accuracy, completeness, or usefulness of any information, apparatus, product, or process disclosed, or represent that its use would not infringe privately owned rights. Reference herein to any specific commercial product, process, or service by trade name, trademark, manufacturer, or otherwise, does not necessarily constitute or imply its endorsement, recommendation, or favoring by the United States Government, any agency thereof, or any of their contractors or subcontractors. The views and opinions expressed herein do not necessarily state or reflect those of the United States Government, any agency thereof, or any of their contractors.

Printed in the United States of America. This report has been reproduced directly from the best available copy.

Available to DOE and DOE contractors from
U.S. Department of Energy
Office of Scientific and Technical Information
P.O. Box 62
Oak Ridge, TN 37831

Telephone: (865) 576-8401
Facsimile: (865) 576-5728
E-Mail: reports@adonis.osti.gov
Online ordering: http://www.osti.gov/bridge

Available to the public from
U.S. Department of Commerce
National Technical Information Service
5285 Port Royal Rd.
Springfield, VA 22161

Telephone: (800) 553-6847
Facsimile: (703) 605-6900
E-Mail: orders@ntis.fedworld.gov
Online order: http://www.ntis.gov/help/ordermethods.asp?loc=7-4-0#online

SAND 2014-1459
Unlimited Release
Printed February 2014

Geomechanical Testing of Bayou Choctaw 102B Core for SPR Analysis

Mathew D. Ingraham, Scott T. Broome, Stephen J. Bauer, Perry C. Barrow and Gregory M. Flint
Geomechanics Department
Sandia National Laboratories
P.O. Box 5800
Albuquerque, NM 87185-0735

Abstract

A laboratory testing program was developed to examine the short-term mechanical and time-dependent (creep) behavior of salt from the Bayou Choctaw Salt Dome. This report documents the test methodologies, and constitutive properties inferred from tests performed. These are used to extend our understanding of the mechanical behavior of the Bayou Choctaw domal salt and provide a data set for numerical analyses.

The resulting information will be used to support numerical analyses of the current state of the Bayou Choctaw Dome as it relates to its crude oil storage function as part of the US Strategic Petroleum Reserve. Core obtained from Drill Hole BC-102B was tested under creep and quasi-static constant mean stress axisymmetric compression, and constant mean stress axisymmetric extension conditions. Creep tests were performed at 100 degrees Fahrenheit, and the axisymmetric tests were performed at ambient temperatures (72-78 degrees Fahrenheit).

The testing performed indicates that the dilation criterion is pressure and stress state dependent. It was found that as the mean stress increases, the shear stress required to cause dilation increases. The results for this salt are reasonably consistent with those observed for other domal salts. Also it was observed that tests performed under extensile conditions required consistently lower shear stress to cause dilation for the same mean stress, which is consistent with other domal salts. Young's moduli ranged from 3.95 x 10^6 to 8.51 x 10^6 psi with an average of 6.44 x 10^6 psi, with Poisson's ratios ranging from 0.10 to 0.43 with an average of 0.30. Creep testing indicates that the BC salt is intermediate in creep resistance when compared with other bedded and domal salt steady-state behavior. The power-law creep relationship for this salt was determined to be:

$$\dot{\varepsilon}_{ss} = 4.08 \times 10^{10} \left(\frac{\Delta\sigma}{\mu} \right)^{4.07}$$

Acknowledgments

The authors would like to acknowledge Byoung Park and Thomas Dewers, Sandia National Laboratories, for their critical review of this report.

Table of Contents

Abstract 3
Acknowledgments 4
Table of Contents 5
List of Figures 6
List of Tables 7
Acronyms and Abbreviations 8
1 Introduction 9
Background 9
Site Description 10
Technical Approach and Scope 12
2 Salt Cores and Specimen Preparation 14
Salt Cores 14
Test Specimens 14
3 Experimental Apparatus and Procedures 16
Mechanical Properties 16
Quasi-static Constant Mean Stress Axisymmetric Compression Tests 16
Quasi-static Constant Mean Stress Axisymmetric Extension Tests 19
Triaxial Compression Constant Stress Creep Tests 19
Calibration 22
4 Results and Analysis 23
Mechanical Properties 23
Density 23
Quasi-Static Triaxial Compression/Extension, Dilation Limit and Deformation Moduli Measurements 24
Creep Behavior 29
5 Summary and Conclusions 35
6 Bibliography 36
Appendix Summary 38
Appendix 1 40
Appendix 2 44
Appendix 3 48

List of Figures

Figure 1: Location of SPR Sites 10
Figure 2: Bayou Choctaw site plan view [Neal et al., 1993] 11
Figure 3. Cross section rendering of Bayou Choctaw dome near Cavern 102 [Neal et al., 1993].....12
Figure 4. Example of salt core cut to length using a wire saw.....15
Figure 5: Image of an instrumented specimen.....17
Figure 6. Testing system used to conduct quasi-static triaxial tests. 18
Figure 7. Sandia-designed creep testing system. 21
Figure 8. Density versus depth for BC Salt (BC-102B), pure Halite has a density of 2.17 g/cc. 24
Figure 9. Dilatant damage criterion of BC salt, BC-102B, represented by the stress invariants: $I_1 = \sigma_1 + \sigma_2 + \sigma_3$ and $\sqrt{J_2} = [\{(\sigma_1 - \sigma_2)^2 + (\sigma_2 - \sigma_3)^2 + (\sigma_3 - \sigma_1)^2\}/6]^{1/2}$. A) Data and fits determined in this study. B) Previous study data compared with fits from this study. 28
Figure 10. Axial strain, radial strain, and axial strain rate versus time histories for a typical creep test (Test 13) of BC salt, BC-102B.....30
Figure 11. Axial creep strain versus time for all Bayou Choctaw creep tests.....31
Figure 12: Example of a creep test (Specimen 19) that underwent uniform deformation. (Sample was cut in half parallel to the core axis).....31
Figure 13. Log steady-state strain rate versus log stress difference for BC salt, BC-102B. 33
Figure 14. Calculated and measured steady-state strain rates for BC salt, BC-102B. 34
Figure 15. BC creep relation in this study versus that of other Gulf Coast domal salts. 34

List of Tables

Table 1. Specimen ID, Test ID, depth and density for all mechanical tests performed. 23
Table 2. Summary of quasi-static triaxial compression/extension tests on BC rock salt, BC-102B.....25
Table 3. Elastic and strength parameters from axisymmetric compression/extension tests on Bayou Choctaw salt, BC-102B. 26
Table 4. Test conditions and results of triaxial compression creep tests on BC rock salt, BC-102B. 29

Acronyms and Abbreviations

ASTM	American Society for Testing and Materials
bgs	Below ground surface
ASC	Axisymmetric Compression
ASE	Axisymmetric Extension
E	Young's moduli
I_1	First invariant of Cauchy stress tensor
J_2	Second invariant of deviatoric stress tensor
LVDT	Linear variable differential transformer
BC	Bayou Choctaw
n	Creep stress exponent
Q	Activation energy
psi	Pounds per square inch
R	Universal gas constant
T	Temperature
$\dot{\varepsilon}_{ss}$	Steady-state strain rate
$\Delta\sigma$	Differential Stress
σ_1, σ_2, σ_3	Principal stresses
σ_{ax}, σ_c	Axial stress, Confining pressure
σ_m	Mean stress
L	Length
D	Diameter
E	Young's modulus
3-D	Three-dimensional

1 Introduction

Background

Sandia National Laboratories, on behalf of The U.S. Department of Energy (DOE), is evaluating the mechanical integrity of the salt pillars surrounding existing petroleum storage caverns in the Bayou Choctaw Dome (Louisiana) that are part of the U.S. Strategic Petroleum Reserve (SPR). The purpose of this experimental effort is to better characterize the salt strength, dilational strength and creep in the salt section above Cavern 102 and below the overlying abandoned caverns, where casing issues have been observed [Park et al., 2006].

The US Strategic Petroleum Reserve (SPR) stores crude oil in 62 caverns located at four different sites in Texas and Louisiana (Figure 1). The reserve contains approximately 700 million barrels (MMB) of crude oil. Some of the caverns were solution mined by the Department of Energy (DOE) and are typified as cylindrical in shape and emplaced at approximately the same depth. The exceptions to this are caverns acquired by the DOE, for example those caverns at Bayou Choctaw (BC). Of the six SPR caverns at BC, five were acquired. The geometry, spacing, and depths of the caverns are irregular. Geotechnical concerns arise due to the close proximity of some of the caverns to each other (e.g., Caverns 15 and 17) or to the edge of salt (e.g., Cavern 20). In addition to the SPR caverns at BC, nine other caverns exist, which store various hydrocarbons and are operated by private industry. Nine abandoned caverns also exist, one of which collapsed (Cavern 7) and another (Cavern 4) is believed to be in a quasi-stable condition [Park et al, 2006].

The core used for this experimental study was obtained from a drill hole from depths encompassing 1068 and 1098 feet below ground surface (bgs), and is above Bayou Choctaw Cavern 102 [Lord et al., 2013]. The top of the salt dome lies between 600 and 700 feet bgs [Park et al., 2006].

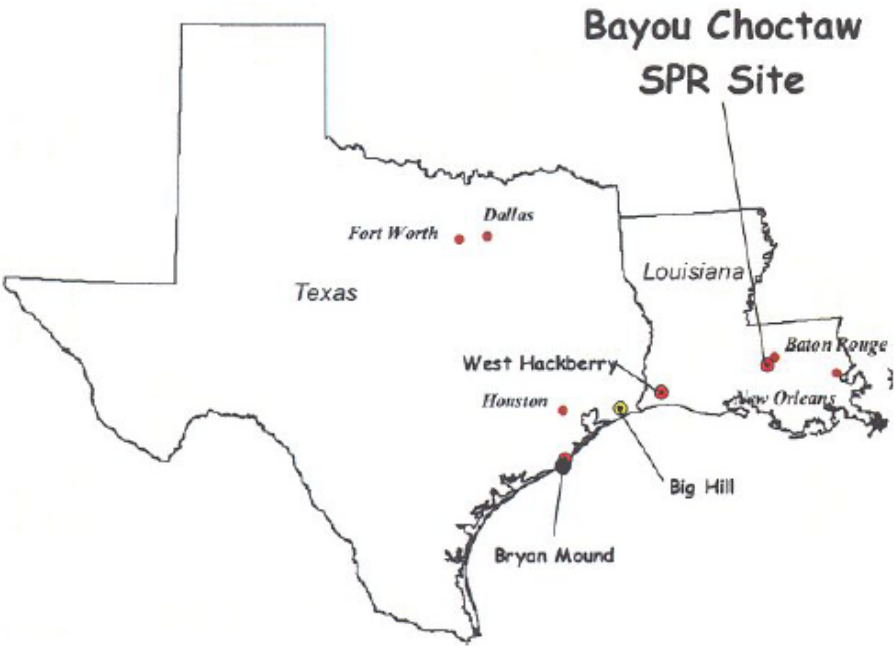

Figure 1: Location of SPR Sites

Site Description

The BC salt dome, located in south-central Louisiana near Baton Rouge (Figure 1), was discovered in 1926. Since then over three hundred oil and gas wells have been drilled on and around the dome, as well as numerous shallow holes drilled into the caprock. Since 1937, Allied Chemical Corporation has drilled over twenty brine wells on the dome. In 1976, the Department of Energy (DOE) purchased eleven of these leached caverns and was storing approximately twenty two million barrels of crude oil in three of the caverns (Caverns 15, 18, and 19), forming part of the Strategic Petroleum Reserve (SPR) Program [Hogan, 1980].

Figure 2 shows a plan view of the BC site with salt contour lines defining the approximate location of the salt dome edge. Of importance to cavern locations and their structural response are the shear zones demarked by contour offsets. The locations of the six SPR caverns, nine UTP (Union Texas Petroleum) caverns, one inactive cavern, and seven abandoned caverns are included.

Figure 3 presents a cross section of the Bayou Choctaw dome showing Cavern 102 with its approximate location with respect to other caverns near that plane through the dome. The well/casing to Cavern 102 must pass through salt pillars separating shallow caverns and the intervening salt which separates shallow from deeper caverns (for example Cavern 102). Also shown is the approximate depth of the core taken for this study.

The top of the BC salt dome lies between 600 and 700 ft bgs. The east flank dips gently downward to 1,500 feet where the dip increases to approximately 80º between 2,000 and 6,000 ft. The west flank of the dome is overhung between 1,000 and 5,000 ft. Below 6,000 to 8,000 ft, the slope of the salt surface diminishes to about 60º [Hogan, 1980].

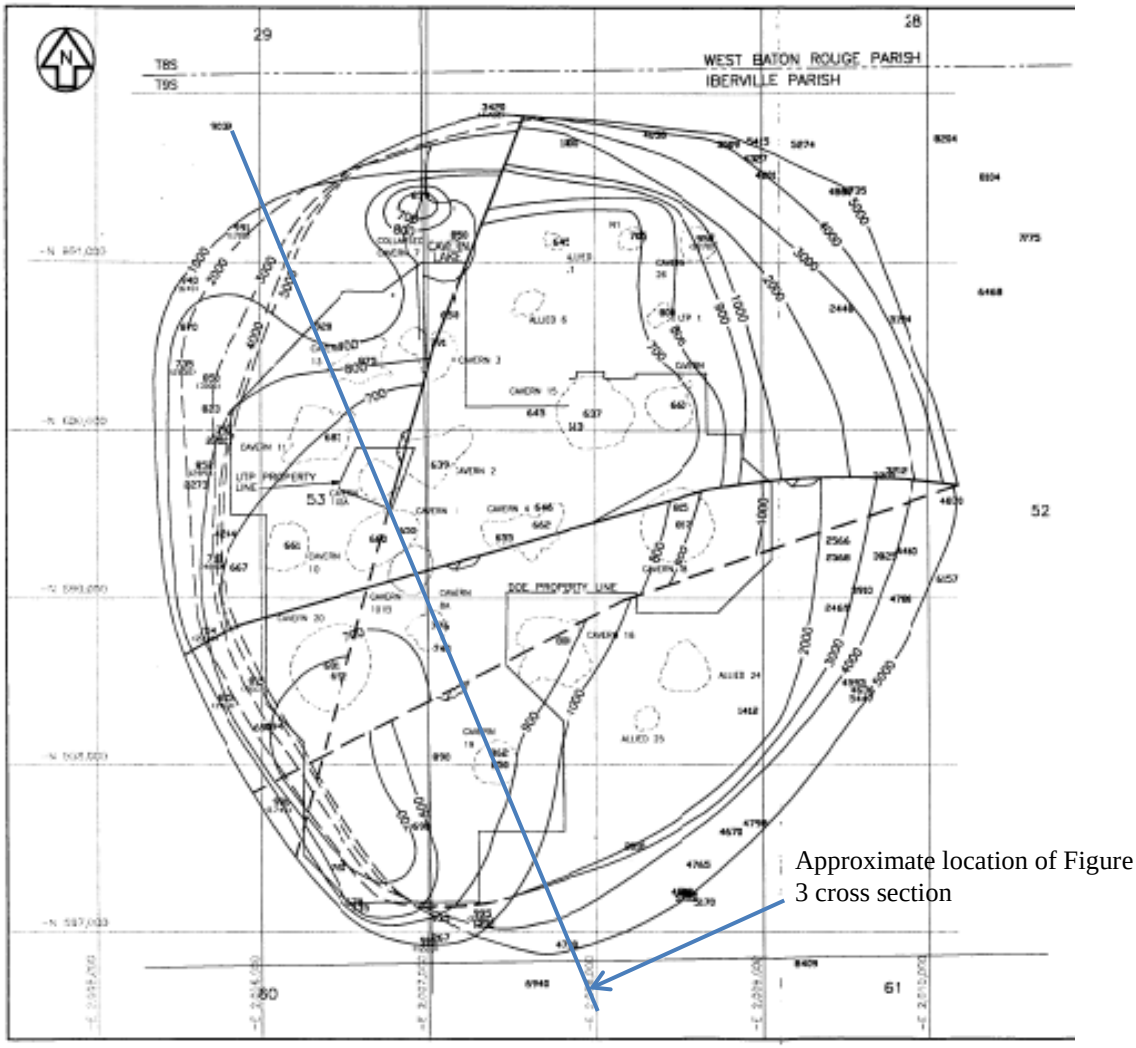

Figure 2: Bayou Choctaw site plan view [Neal et al., 1993]

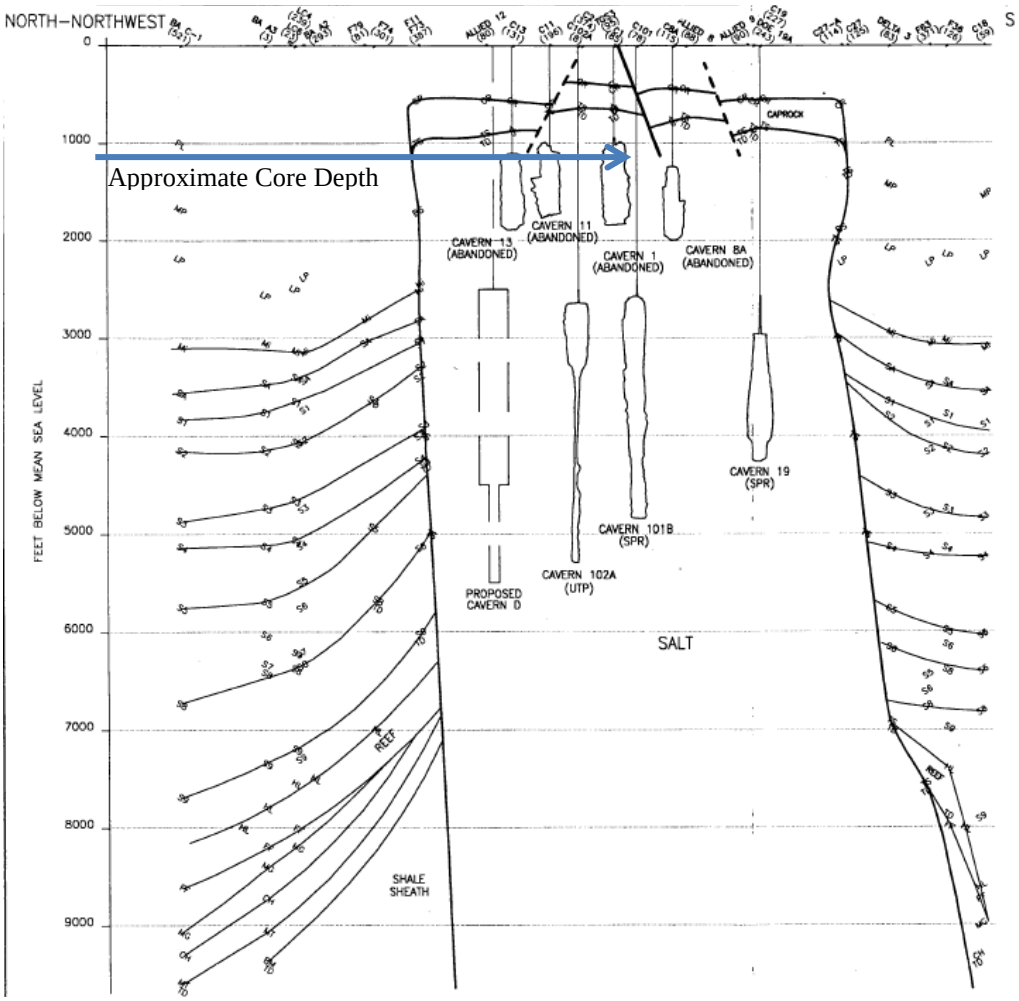

Figure 3. Cross section rendering of Bayou Choctaw dome near Cavern 102 [Neal et al., 1993].

Technical Approach and Scope

Natural rock salt deposits are used for storage of crude oil because of their low permeability (good for containment), ease of mining, and proximity to shipping and refining operations.

The mechanical behavior of rock salt is unique when compared with other geologic media. Salt is well known to demonstrate significant time dependent deformation in the absence of fracturing when subjected to non-hydrostatic stresses [ex. DeVries et al 2003]. This can result in cavern closure over time resulting in reduced volume for storage. This is evaluated using standard creep tests [ex. DeVries et al 2003]. Salt is also known to dilate under loading due to stress-induced microfracturing under different stress states [Munson et al, 2003]. Elastic properties and dilation behavior were determined using axisymmetric extension and compression tests [ex. DeVries et al 2003]. Comparison with available published data of other rock salts is presented in the results section. All testing performed on the BC 102 salt core was recovered from a continuous core run at a depth of 1068 to 1098 feet bgs.

The report is organized as follows. Specimen handling and specimen preparation are first described, followed by explanation of experimental apparatus and experimental processes. Mechanical properties results and analysis of those results precludes the conclusion of the report. Each section includes a summary and comparison to other relevant data sets where appropriate. Appendices provide the detailed results from each specimen.

2 Salt Cores and Specimen Preparation

Salt Cores

The salt in this experimental study was taken from the BC-102B drill hole into the Bayou Choctaw Salt Dome in Louisiana. The core is from above an existing storage cavern and is from a depth of 1070-1098 feet bgs. The composition of the tested salt was not quantitatively confirmed in this study. Visual observation of the salt finds the salt to be relatively pure halite with less than 2% impurities by volume, specimens from higher in the core appeared darker which implies they may have 1-2% more impurities [Lord et al., 2013].

Test Specimens

Specimens for the axisymmetric compression and creep testing, approximately 4 inches in diameter and 8 inches in length, were made using the as-received core diameter. These specimens were cut to an approximate length on a band saw or wire saw (depending on how close to a core end the cut needed to be made, see Figure 4). The ends were ground on a surface grinder equipped with a sanding wheel to ensure that the ends of the specimen were parallel and perpendicular to the core axis.

Specimens for the axisymmetric extension testing measured approximately 2.75 inches in diameter and 5.5 inches in length. This specimen size was necessary because the piston of the pressure vessel used for testing is 3 inches in diameter; for extension testing the specimen diameter must be smaller than the piston diameter to achieve the necessary stress state.

The smaller specimens were made by subcoring the 4 inch core to approximately 3 inches. To ensure roundness of the specimens, these were turned down on a lathe to a diameter of 2.75 inches. As before, these specimens were ground on a surface grinder using a sanding wheel. Surface grinding for both geometries resulted in a surface with a parallelism tolerance of 0.001 inches per inch of specimen diameter as per ASTM standard D-4543 [ASTM, 1995].

Any imperfections (e.g. plucked grains) in the surface of the specimens were filled with Ultracal® plaster. This was done to ensure that confining jackets would not rupture due to a void in the specimen. After the specimens were prepared, they were stored in a 50°C oven for at least 48 hours prior to testing to ensure removal of adsorbed water. Prior to testing, initial specimen density was calculated using the weight of the specimens and calculated specimen volume (assumed a perfect right circular cylinder). Density, depth, and testing type are summarized in Table 1.

Before jacketing the specimens, the ends were lubricated with a 50/50 mixture by weight of stearic acid and petroleum jelly [Labuz and Bridell, 1993]. A half inch tall ring of Viton was then placed around the top and bottom of the specimen-end cap interface to cover this area and mitigate leak potential. Once this was done the end caps were placed on the specimen, and jackets were applied to isolate the specimen from confining fluid. For creep tests, a Viton jacket was used, which was sealed to the end caps using O-rings and tie-wire. For the axisymmetric

compression and extension tests, polyvinyl chloride (heat shrink) tubing was used, and was again sealed to the end caps with O-rings and tie-wire.

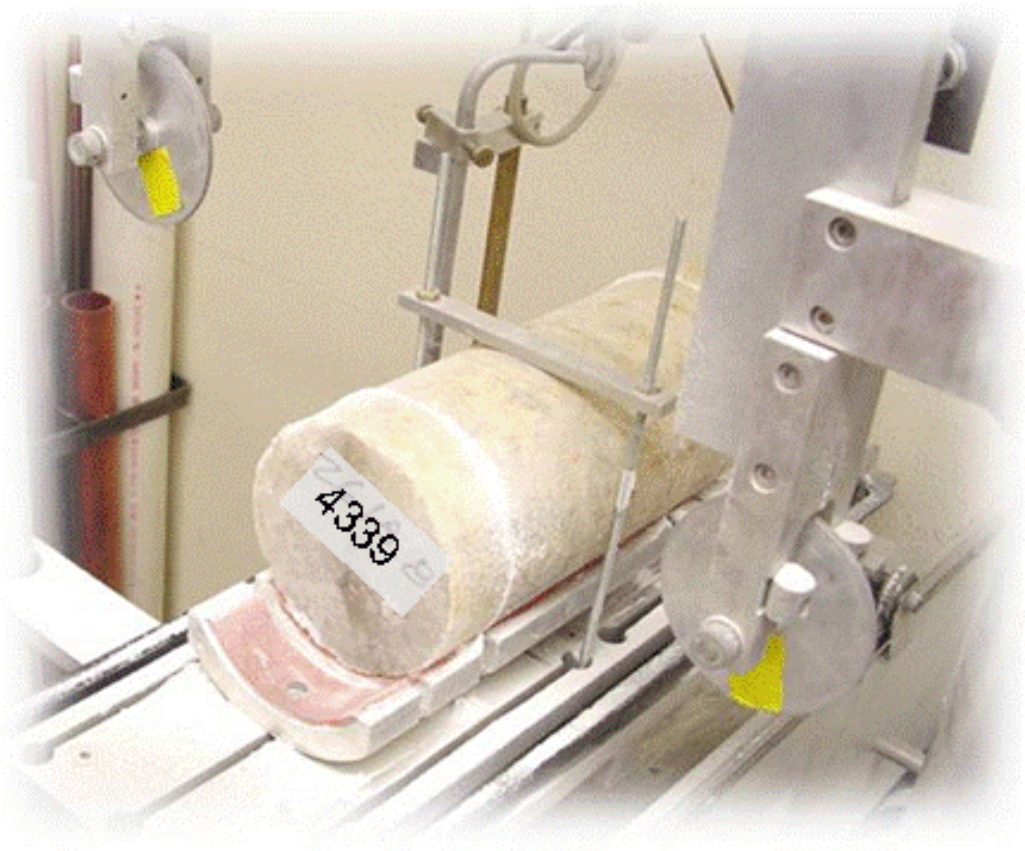

Figure 4. Example of salt core cut to length using a wire saw.

Prior to testing, all axisymmetric compression and extension constant mean stress specimens were conditioned in the test fixture at a hydrostatic pressure of 5000 psi for at least 12 hours at room temperature. This step was performed to condition the salt such that the grains at their boundaries are pushed together and generates a more consistent and representative test of the core [e.g. Lee et al., 2004, Broome et al., 2009]. For the creep tests the specimens were conditioned at 1100 psi and 100 degrees F, the creep test conditions for at least 12 hours.

3 Experimental Apparatus and Procedures

Mechanical Properties

The mechanical testing consisted of three different test series: 1) quasi-static constant mean stress axisymmetric compression tests 2) quasi-static constant mean stress axisymmetric extension tests, and 3) axisymmetric triaxial compression constant differential stress creep tests.

Quasi-static Constant Mean Stress Axisymmetric Compression Tests

Constitutive properties of pressure sensitive materials such as rock are often determined using axisymmetric compression tests. These are typically either constant mean stress or constant confining stress. For the constant mean stress tests performed in this study the mean stress (sum of the three principal stresses divided by three) is held constant after the desired mean stress is reached following hydrostatic loading. For a system such as this where the intermediate and minimum principal stresses are equal, for every increment of the maximum principal stress increases (axial, parallel to the central axis), the confining pressure decreases by half of the increment. The effect of the mean stress is evaluated by performing tests at a number of different mean stresses spanning the range of interest.

Test specimens were instrumented to measure axial and radial displacements during application of the initial hydrostatic pressure, and during the axial compression (shear loading) portion of the test. Displacements were measured with Linear Variable Differential Transformers (LVDTs). Two LVDTs were mounted on the end caps to measure the axial deformation, and two were mounted in a ring placed around the midheight of the specimen to measure the change in diameter, the averages of these values were used to calculate strains. Figure 5 shows an instrumented specimen. The dilation stress (volume expansion of the rock resulting from microcracking) of the specimen may be determined by calculating the volume strain from the axial and radial strain values, determined from displacement measurements. Stress-strain data were also used to evaluate mechanical properties such as elastic moduli.

Figure 6 shows an example of the computer-controlled servo-hydraulic testing system used to conduct the axisymmetric tests at ambient temperature. The system consists of an MTS reaction load frame, coupled with an SBEL (Structural Behavior Engineering Laboratory) pressure vessel. The pressure vessel housing the test specimen was connected to a pressure intensifier capable of inducing pressures up to 30,000 psi. Isopar® is used as the confining medium. The reaction frame has a movable crosshead to accommodate pressure vessels of different sizes and configurations. The frame used is capable of applying loads up to 220,000 pounds through a hydraulic actuator in the base of the frame. Vessel pressures were measured with a pressure transducer plumbed directly into the hardline that connects the pressure vessel to the pressure intensifier. The transducer is located about 5 ft from the vessel pressure. Axial forces were measured with a load cell attached to the reaction frame outside of the pressure vessel.

Setup of the tests began by placing the jacketed and instrumented specimen into the base of the pressure vessel and making the electrical connections to feed-throughs in the pressure vessel,

assembling the pressure vessel and placing it into the reaction frame. The actuator in the base of the frame is raised gradually to bring the pressure vessel piston into contact with the reaction frame. The pressure vessel is then connected to the pressure intensifier and filled with Isopar®. At this point the servohydraulic control is turned on and data collection begins. The confining pressure is raised to 5000 psi, with the reaction frame actuator holding its position. After maintaining this condition for >12 hours at 5000 psi, the confining pressure was reduced to the desired mean stress. Subsequently, the following steps were performed in order to conduct the test:

1) Hydrostatic pressure was lowered from conditioning pressure until the desired constant mean stress was reached
2) An axial unload –load cycle was performed at constant confining pressure so that Young's Modulus could be determined.
3) The constant mean stress test was begun, which entailed increasing the axial load in displacement control (approximating $5x10^{-5}$ sec^{-1} strain rate) while decreasing the confining pressure such that the mean stress remained constant
4) Unload –load cycles were performed under constant mean stress conditions at the discretion of testing personnel throughout the test.
5) Tests were run until dilation was apparent using active real time determination of volume strain or until a jacket leak occurred.
6) Tests were ended by returning to a hydrostatic condition, followed by a lowering of confining pressure.

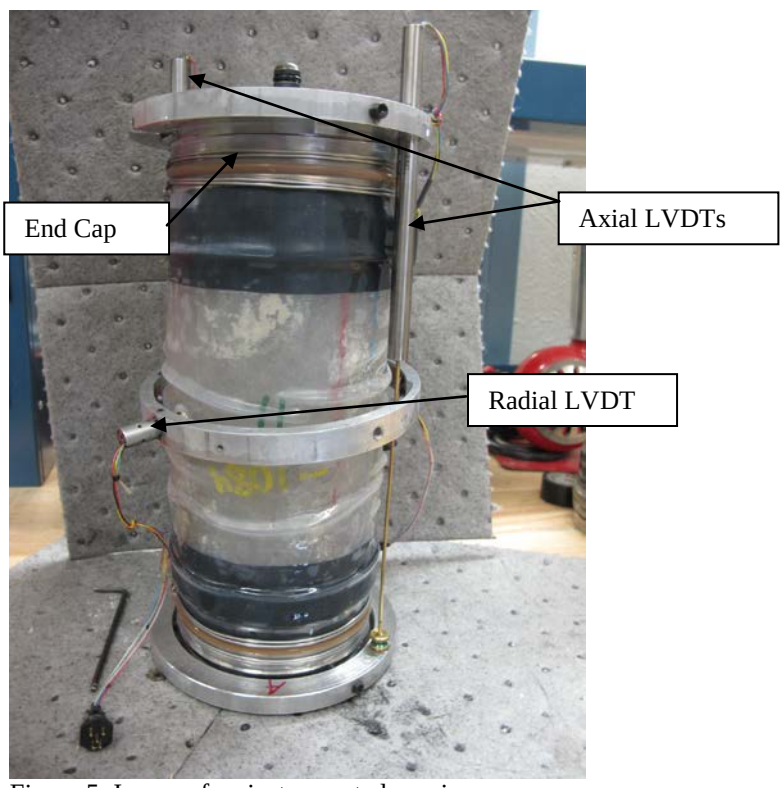

Figure 5: Image of an instrumented specimen.

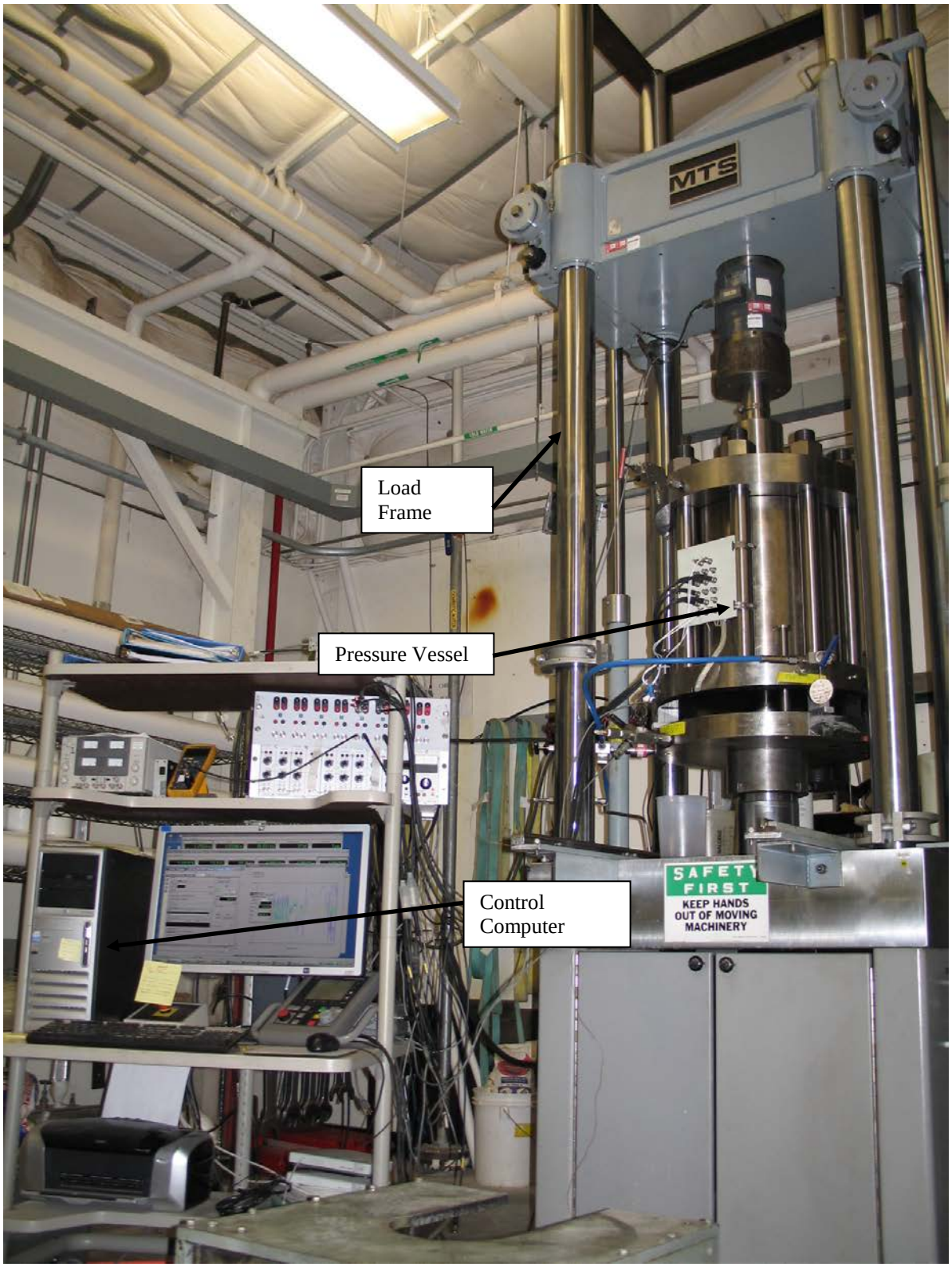

Figure 6. Testing system used to conduct quasi-static triaxial tests.

Quasi-static Constant Mean Stress Axisymmetric Extension Tests

The axisymmetric extension tests were largely similar to the axisymmetric compression tests. Jacketing and instrumentation of the specimens was the same, and the specimens were tested in the same pressure vessel and reaction frame. However, there were some critical differences. First the specimens are 2.75 inches in diameter in order to attain a specimen size/geometry compatible with the test system and able to generate the desired stress state. The calculation for mean stress is the same as in the axisymmetric compression tests, however in the extension tests the axial load is decreased in displacement control (approximately 1.5×10^{-5} sec^{-1} strain rate) while the confining pressure was increased to maintain the constant mean stress condition. During extension, for every increment the axial stress decreases, the confining stress increases by half that increment.

It is also necessary to seal the specimen to the pistons with a ring to isolate the piston and the end of the specimen from confining pressure, allowing decoupling of the axial and confining pressures. Otherwise it is not possible to release axial load. To ensure this seal during the hydrostatic portion of the test, a stress of 300 psi over hydrostatic pressure was maintained axially on the specimen during the hydrostatic portion of loading only. Similar to the axisymmetric compression tests, the goal of the axisymmetric extension tests is to determine the onset of dilation. Tests are run until dilation is seen, or the jacket leaks. Jacket leaks are common for these tests when the axial stress becomes low. Typically around 600 psi axial, the seal attaching the specimen to the piston fails or a jacket ruptures. This is due to insufficient load on the specimen to maintain the seal. As with axisymmetric compression tests, unload – reload loops were performed to evaluate elastic parameters during the tests. Elastic parameters were determined from the reload portion of the unload-reload loops performed during testing.

Triaxial Compression Constant Stress Creep Tests

Time-dependent behavior of BC salt was determined through a series of triaxial compression constant stress creep tests. These are similar to the axisymmetric compression tests performed. However, they are performed at constant confining pressure, and at a constant axial stress instead of a constant displacement rate. As with the axisymmetric compression/axisymmetric extension tests the specimen is initially loaded hydrostatically. Then the constant axial stress difference (axial stress minus confining pressure), is applied and the deformation of the specimen is measured as a function of time. Creep deformation of salt is highly dependent on both the magnitude of the applied stress difference and the temperature at which the test is conducted. Therefore, typically a test series is performed at different axial stresses and temperatures. However, due to the small number of specimens available only one temperature was tested in this series. The temperature and confining pressure at which the tests were performed is representative of the conditions at the depth the core was collected.

Figure 7 shows a typical Sandia-designed creep testing system [Broome et al., 2009]. It consists of a reaction frame that generates the axial force by reacting against a hydraulic cylinder located at the base of the frame, and a pressure vessel that houses specimens during testing. The reaction frame system is capable of applying loads of up to 100,000 pounds. The pressure vessel is rated to 10,000 psi and is equipped with electrical band heaters capable of maintaining test temperatures up to approximately 450 degrees Fahrenheit. Silicon oil is used as the confining medium. Axial loads are adjusted using an air-assisted pump and vessel pressures can be

maintained constant using a dilatometer system that either injects or withdraws oil from the vessel. Vessel pressures are measured by a pressure transducer plumbed into the hydraulic line leading from the vessel to the dilatometer. Axial loads applied by the hydraulic cylinder are measured by a load cell located directly above the cylinder in line with the axial push-rod that extends into the pressure vessel and applies axial load to the ends of the specimen. Test temperature is recorded by two thermocouples, one located near the top of the pressure vessel and other near the vessel midheight. Specimens are vented to atmospheric pressure during testing.

To begin testing the specimen assembly was placed inside the pressure vessel, which was then filled with silicon oil. The pressure in the vessel was increased to the target level (1,100 psi for all the creep tests in this study) and allowed to stabilize. The vessel was then heated to the target temperature by activating band heaters located on the outside of the pressure vessel and either clamped to or housed inside the piston. The temperature was allowed to stabilize for approximately 24 hours. After temperature stabilization was completed, the target stress difference was applied by rapidly increasing the axial load (inside of about 30-60 seconds) on the specimen using the hydraulic cylinder. When the target load was reached, control of the test was turned over to an Azonix controller that maintained constant axial stress and constant confining pressure throughout the duration of the test and also served as the data acquisition system. Because salt specimens undergo rather large radial expansion during testing, the axial force applied to the ends of the specimen was automatically adjusted (increased) based on the long range external LVDT reading (assuming a constant volume of the specimen) to account for the change in specimen cross-sectional area, thereby ensuring constant stress (rather than constant force) conditions were maintained. The creep tests were terminated when the strain rate reached a constant steady-state value or was changing so slowly it could not be discerned. The test durations were typically >50 days.

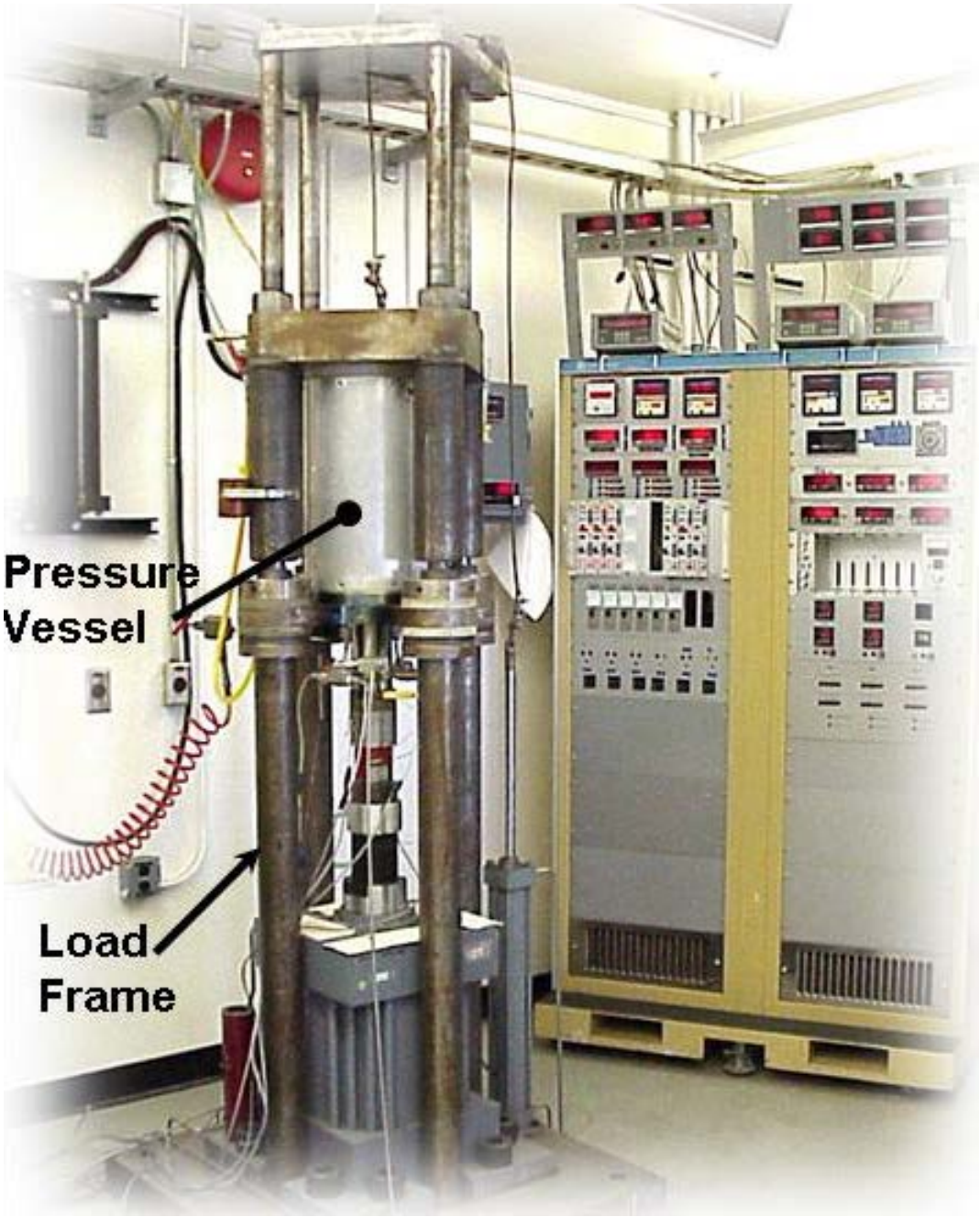

Figure 7. Sandia-designed creep testing system.

Creep deformations were measured by electronic transducers mounted inside and outside the pressure vessel. Axial deformation was measured by a pair of internal LVDTs (1.0 inch) as well as two independent LVDTs within their linear range (0.1 inch and 1.0 inch) that tracked the displacement of the axial push-rod relative to the bottom of the pressure vessel. This displacement was a direct measure of the axial displacement of the specimen because non-specimen deformations were negligible given the imposed constant stress condition. The external LVDTs were mounted 180º apart on the push-rod. During the tests, the 0.1-inch-range

LVDTs were reset periodically when the range was exceeded. Radial displacements were measured directly with a Schueler gage mounted on the specimen.

Calibration

Data collected in the experimental study included force, pressure, temperature, displacement, and volume change. Typically, these data are acquired using electronic transducers in which the electrical output is proportional to the change in the measured variable. In all cases, the constants of proportionality were determined through careful calibration using standards traceable to the National Institute for Standards and Technology.

4 Results and Analysis

Mechanical Properties

The mechanical properties testing comprised three test series: 1) quasi-static constant mean stress axisymmetric compression (ASC) tests; 2) quasi-static constant mean stress axisymmetric extension (ASE) tests and 3) triaxial compression constant stress creep tests. These are summarized in Table 1 below:

Table 1. Specimen ID, Test ID, depth and density for all mechanical tests performed.

Specimen ID	Test ID	Depth (ft)	Density (g/cc)
1	Creep	1070.2	2.151
2	ASC	1069.6	2.163
3	ASE	1068.9	2.160
4	Creep	1078.6	2.149
5	ASC	1077.9	2.158
6	ASE	1077.4	2.162
7	Creep	1080	2.152
8	ASC	1080.7	2.154
9	ASE	1081.5	2.160
10	Creep	1083	2.158
11	ASC	1083.7	2.155
12	ASE	1084.4	2.155
13	Creep	1089	2.153
14	ASC	1089.7	2.155
15	ASE	1090.8	2.159
16	Creep	1092.5	2.141
17	ASC	1093.2	2.154
18	ASE	1093.9	2.147
19	Creep	1095.9	2.153
20	ASC	1096.6	2.163
21	ASE	1097.5	2.156

Density

Density was determined by dividing the mass of the specimen by the calculated volume. The volume was calculated by measuring the length and diameter of the specimen and assuming a perfect right circular cylinder. Figure 8 plots the specimen density relative to its depth and shows that the rock salt density over this depth interval has some variation but is within 1.5% of pure halite.

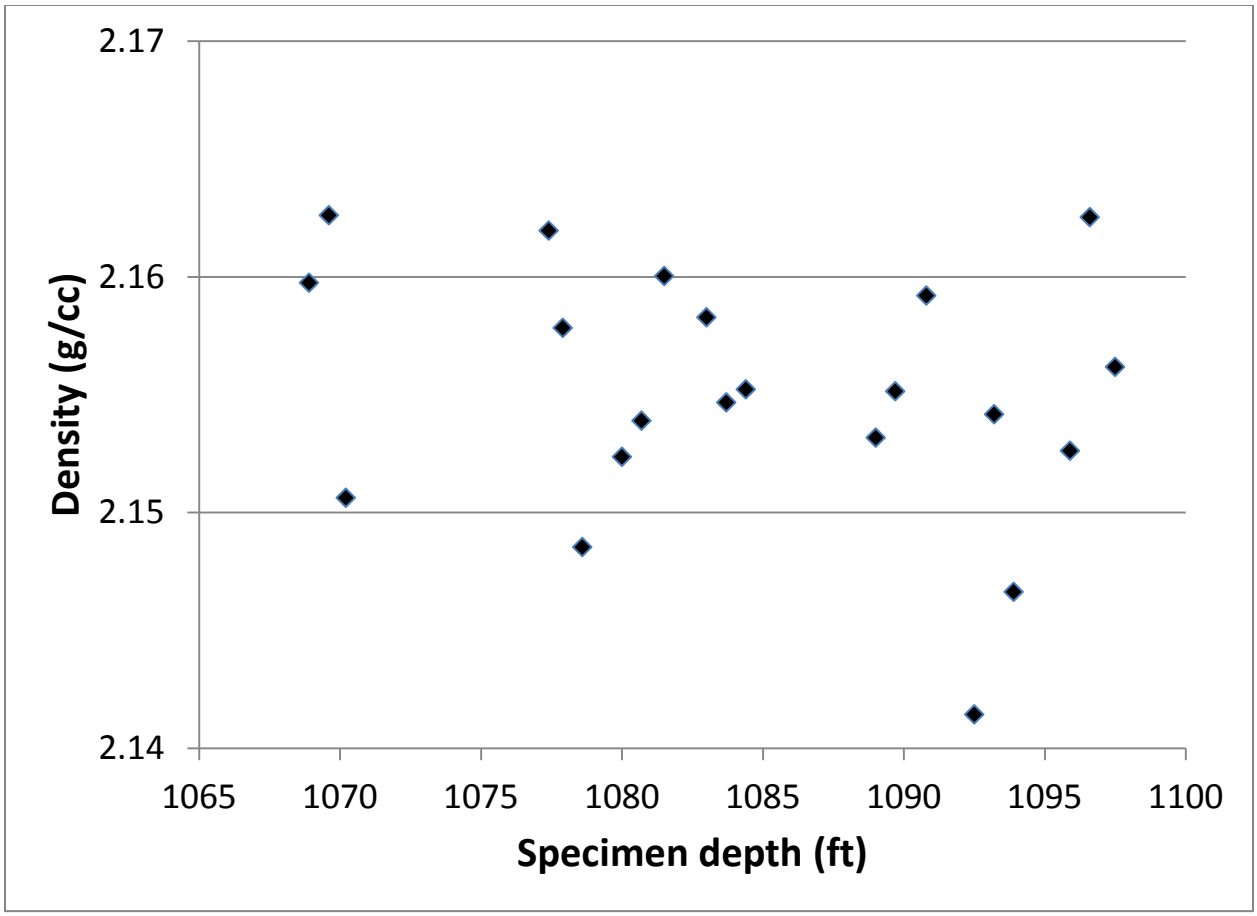

Figure 8. Density versus depth for BC Salt (BC-102B), pure Halite has a density of 2.17 g/cc.

Quasi-Static Triaxial Compression/Extension, Dilation Limit and Deformation Moduli Measurements

Seven axisymmetric compression tests and seven axisymmetric extension tests were performed on rock salt cores from approximately 1065-1100 ft bgs to determine dilational compressive strengths and static elastic properties. Table 2 summarizes certain key results for the quasistatic testing. Appendix 1 and 2 provides stress difference versus axial, lateral and volumetric strains for each of the fourteen triaxial tests. It should be noted that compression tests specimens 5, 11, and 14 were wet with confining fluid after testing. This could be due to a jacket leak during the test rendering these strength data unreliable and unusable. Because salt has low permeability it may not be possible to discern a jacket leak during testing. If a leak did occur it would aberrate the mechanical response from the desired conditions. Leaks are suspected in these three specimens and while they are included in data tables they are excluded from analysis used to determine the dilation criteria.

Leaks also occurred with specimens 9 and 21 (axisymmetric extension). Therefore we include the data in tables but exclude it from analysis of dilation limits. These tests were used for elastic property determinations as data collected prior to leaking is valid. It was known that these

specimens leaked because in the extensile stress state a leak caused a sudden pressure drop when fluid came through the pore pressure ports of the vessel indicating that the ends of the specimen were no longer sealed.

The dilation stress was defined as the von Mises equivalent shear stress level at the minimum specimen volume (i.e. when the strain changed from compactant to dilatant). The sign convention is used such that dimensional decreases are positive and volume decreases are positive while dimensional increases are negative and volume increases are negative.

Table 2. Summary of quasi-static triaxial compression/extension tests on BC rock salt, BC-102B.

Test no.	Test type	Depth top	Mean Stress, P (σ_3 initial)	σ_{diff}	$\sigma_{1,d}$	$\sigma_{3,d}$	$I_{1,d}$	$J_2^{0.5}{}_{,d}$
		(ft)	(psi)	(psi)	(psi)	(psi)	(psi)	(psi)
1	Creep	1070.2	1100	1500				
2	ASC	1069.6	1533		2280	1159	4598	1660
3	ASE	1068.9	4308		1409	5789	12923	2518
4	Creep	1078.6	1100	1000				
5+	ASC	1077.9	3625		3969	3264	10875	639
6	ASE	1077.4	3002		932	4035	9005	1792
7	Creep	1080	1100	2000				
8	ASC	1080.7	5665		7182	3264	16995	4157
9	ASE	1081.5	3795		*	*	11384	*
10	Creep	1083	1100	2750				
11+	ASC	1083.7	3970		4581	3725	11906	931
12	ASE	1084.4	5095		1156	7066	15286	3361
13	Creep	1089	1100	3250				
14+	ASC	1089.7	2870		3258	2485	8613	883
15	ASE	1090.8	4470		2213	5233	13407	1278
16	Creep	1092.5	1100	3750				
17	ASC	1093.2	2350		6579	236	7051	3661
18	ASE	1093.9	3715		4994	3612	11136	2581
19	Creep	1095.9	1100	5850				
20	ASC	1096.6	2215		4818	916	6642	2182
21	ASE	1097.5	2330		*	*	6990	*

*specimen leaked during the extensile portion of the test, no dilation data could be obtained.
+specimen data was not used for developing dilation envelope

Static Elastic Moduli: Static elastic moduli determined from the unload – reload data acquired during the quasi-static constant mean stress compression/extension tests are summarized in Table 3. The static elastic Young's modulus, E_{static}, was determined directly from the slope of the unload/reload stress difference versus axial strain curve. Values of static elastic Poisson's ratio were calculated from the ratio of E_{static} to the slope of the unload/reload stress difference versus

lateral strain curve. Young's modulus ranges from approximately 3.95 x 10^6 to 8.51 x 10^6 psi with an average of 6.44 x 10^6 and generally increased with increasing mean stress. Poisson's ratio ranges from approximately 0.10-0.43 with an average of 0.30.

Table 3. Elastic and strength parameters from axisymmetric compression/extension tests on Bayou Choctaw salt, BC-102B.

Test no.	Test type	Depth top	Mean Stress, P (σ_3 initial)	$I_{1,d}$	$J_2^{0.5}{}_{,d}$	Young's Modulus,E	Poisson's Ratio
		(ft)	(psi)	(psi)	(psi)	psi x10^6	
2	ASC	1069.6	1533	4598	1660	4.37	0.10
3	ASE	1068.9	4308	12923	2518	8.51	0.34
5+	ASC	1077.9	3625	10875	639	3.95	0.24
6	ASE	1077.4	3002	9005	1792	6.65	0.24
8	ASC	1080.7	5665	16995	4157	7.79	0.30
9	ASE	1081.5	3795	11384	*	6.38	0.38
12	ASE	1084.4	5095	15286	3361	7.37	0.29
15	ASE	1090.8	4469	13407	1278	6.54	0.33
18	ASE	1093.9	3712	11136	2581	8.12	0.43
20	ASC	1096.6	2215	6642	2182	4.12	0.27
21	ASE	1097.5	2330	6990	*	7.01	0.37
Average						6.44	0.30

*specimen leaked during the extensile portion of the test, no dilation data could be obtained.
+specimen data was not used for developing dilation envelope

Dilational Strength: The dilational strength used in this report is the shear stress level at the minimum specimen volume. This is defined as the point at which the volume strain changes from compactant to dilatant, as determined from the stress – strain data collected. This definition is consistent with the literature [Mellegard and Pfeifle, 1994]. Table 2 summarizes the dilational strength results from our laboratory experimental program of BC salt consisting of seven axisymmetric compression tests and seven axisymmetric extension tests. Test parameters for the seven creep tests are also listed in Table 2.

The stress states that produce dilation of pressure-dependent materials are often expressed in terms of two stress invariants, i.e., the first invariant of the Cauchy stress tensor, I_1, and the second invariant of the deviatoric stress tensor, J_2. These two invariants are defined mathematically as:

$$I_1 = \sigma_1 + \sigma_2 + \sigma_3 \qquad \textbf{Eq. 1}$$

$$J_2 = \frac{1}{6}\left\{(\sigma_1 - \sigma_2)^2 + (\sigma_2 - \sigma_3)^2 + (\sigma_3 - \sigma_1)^2\right\} \qquad \textbf{Eq. 2}$$

where σ_1, σ_2, and σ_3 are the maximum, intermediate, and minimum principal stresses, respectively. The experimental dilational strengths are plotted in Figure 9. In Figure 9A, we

present the BC dilatational strength data, plotted in I_1 versus $\sqrt{J_2}$ space, this line is defined by the equation $\sqrt{J_2} = 16902 - 16595e^{-.00001039 I_1}$ for the extension tests, and $\sqrt{J_2} = 70575 - 69605e^{-.00000255 I_1}$ for the compression tests [Lee et al., 2004]. These fits are reasonable and make sense for the size of the data set used to generate them. The ASC fit is above the ASE fit as expected. In Figure 9B the ASC fit is compared to existing data sets from the Richton and Big Hill SPR sites as well as the Van Sambeek criteria [Van Sambeek et al., 1993, Lee et al., 2004, Broome et al., 2009].

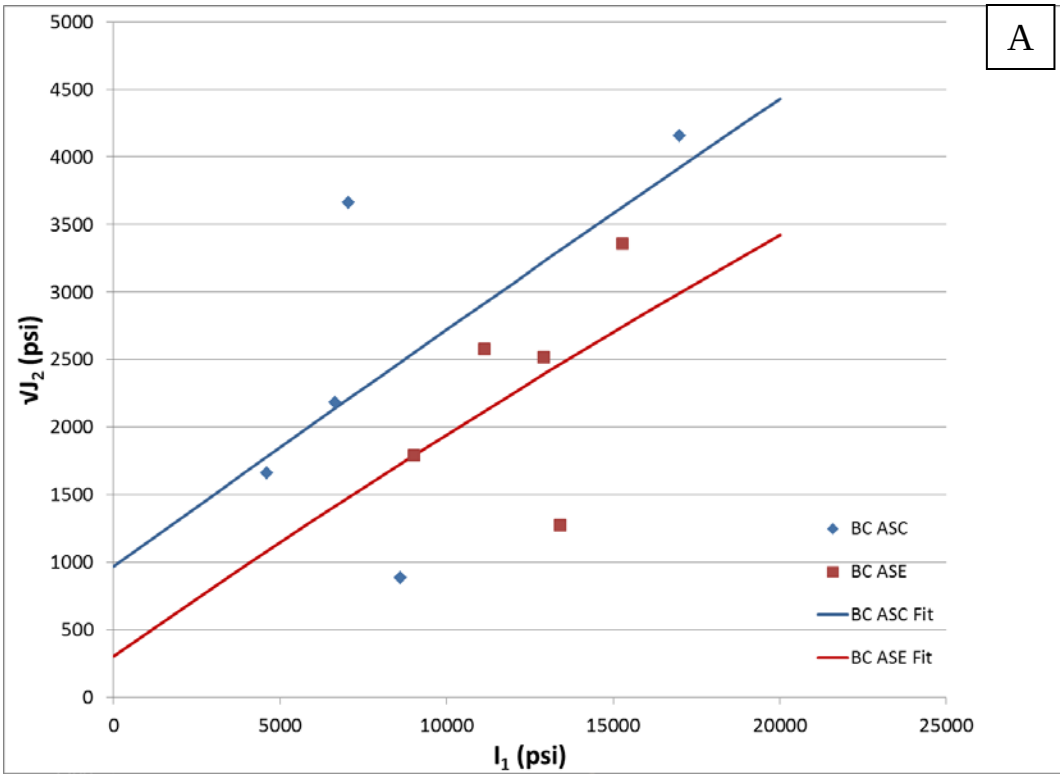

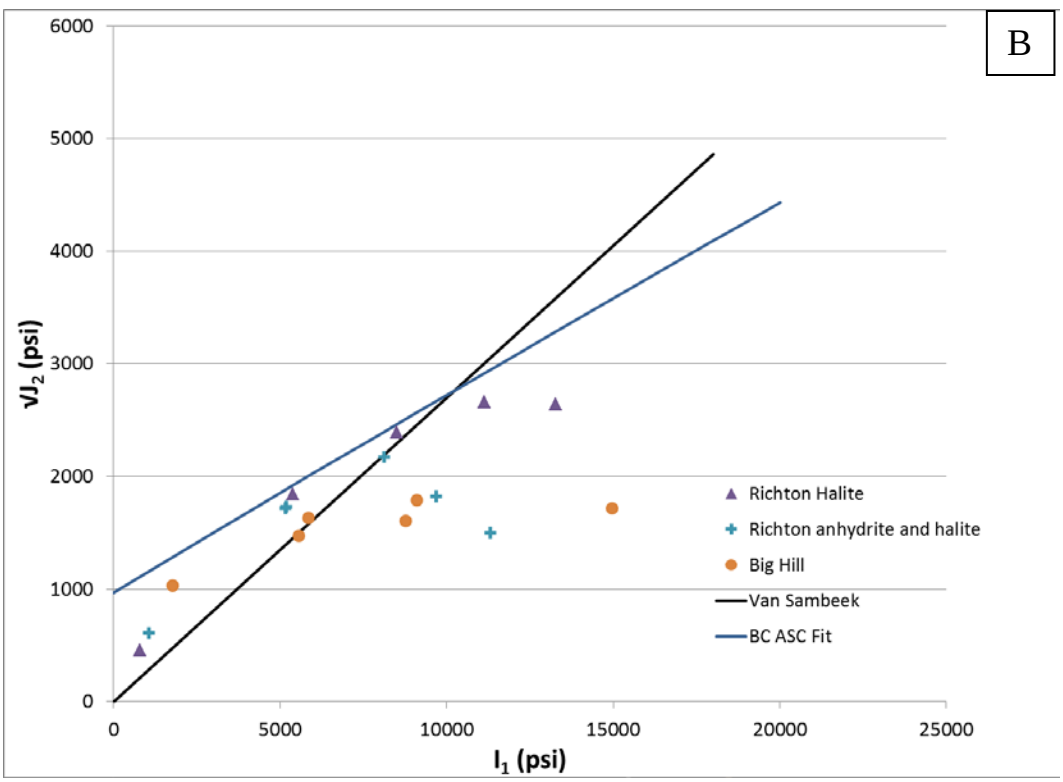

Figure 9. Dilatant damage criterion of BC salt, BC-102B, represented by the stress invariants: $I_1 = \sigma_1 + \sigma_2 + \sigma_3$ and $\sqrt{J_2} = [\{(\sigma_1 - \sigma_2)^2 + (\sigma_2 - \sigma_3)^2 + (\sigma_3 - \sigma_1)^2\}/6]^{1/2}$. A) Data and fits determined in this study. B) Previous study data compared with fits from this study.

Creep Behavior

A total of seven creep tests were performed on BC salt. All tests were conducted at a confining pressure of 1,100 psi, temperature of 100°F, and at stress differences ranging from 1,053 to 5,647 psi (Table 4). The values of temperature and confining pressure were chosen as representative of the in situ conditions of the salt.

Figure 10 plots axial, radial, and volumetric strains versus time and axial strain rate versus time for Test I.D. 13, as an example.. The three axial strain curves represent the output from three independent measurements of axial deformation – one using a lower range LVDT (0 to 0.1 inches), one using a higher range LVDT (0 to 1.0 inches), and one using a pair of internal LVDTs (0 to 1.0 inch range). Both the axial and radial strain curves are typical of rock salt in that the strain rates are high initially but then decrease monotonically to a constant or nearly constant value over time. In this example, strain rate reaches a constant value (~4.94×10^{-9} s^{-1}) between 50 and 56 days. Similar plots are provided in Appendix 3 for each of the seven creep tests. Plots of stress difference, confining pressure, and temperature are also shown in Appendix 3 for each test.

Axial strain for each of the seven creep tests is plotted in Figure 11. The respective curves are well ordered in that the smallest strains are seen for the lowest stress difference magnitudes. The experimental value for axial strain rate was calculated from the slope of the axial strain vs. time data using the linear-least squares method. For most tests approximately the last five days of axial strain data were used from each creep test to determine the measured axial (steady-state) strain rate. The highest stress difference test only ran for 4 days and the axial strain rate was determined from the last few hours of test data, this represents a similar time fraction for this test, as compared with the longer tests. This method for estimation of steady state creep is based of a percentage of total test time and empirical experience.

Table 4. Test conditions and results of triaxial compression creep tests on BC rock salt, BC-102B.

Test I.D.	Recovery Depth (feet)	Stress Difference (psi)	Temperature (°F)	Test Duration (days)	Final Axial Strain Rate measured (s^{-1})	Final Axial Strain Rate calculated (s^{-1})
1	1070.2	1428	100	58	7.37E-10	6.52E-10
4	1078.6	1053	100	78	1.18E-10	1.89E-10
7	1080	1948	100	70	9.98E-10	2.31E-09
10	1083	2736	100	56	5.86E-09	9.18E-09
13	1089	3226	100	57	4.94E-09	1.80E-08
16	1092.5	3725	100	36	9.14E-09	3.22E-08
19	1095.9	5647	100	4	2.81E-07	1.75E-07

Confining pressure = 1100 psi in all tests.

An example of the uniform deformation of the salt experiencing high deformation is shown in Figure 12 (Test 19). Here the specimen was shortened 27% axially and exhibits fairly uniform

deformation, typified by uniform axial shortening and lateral expansion with some barreling of the sample.

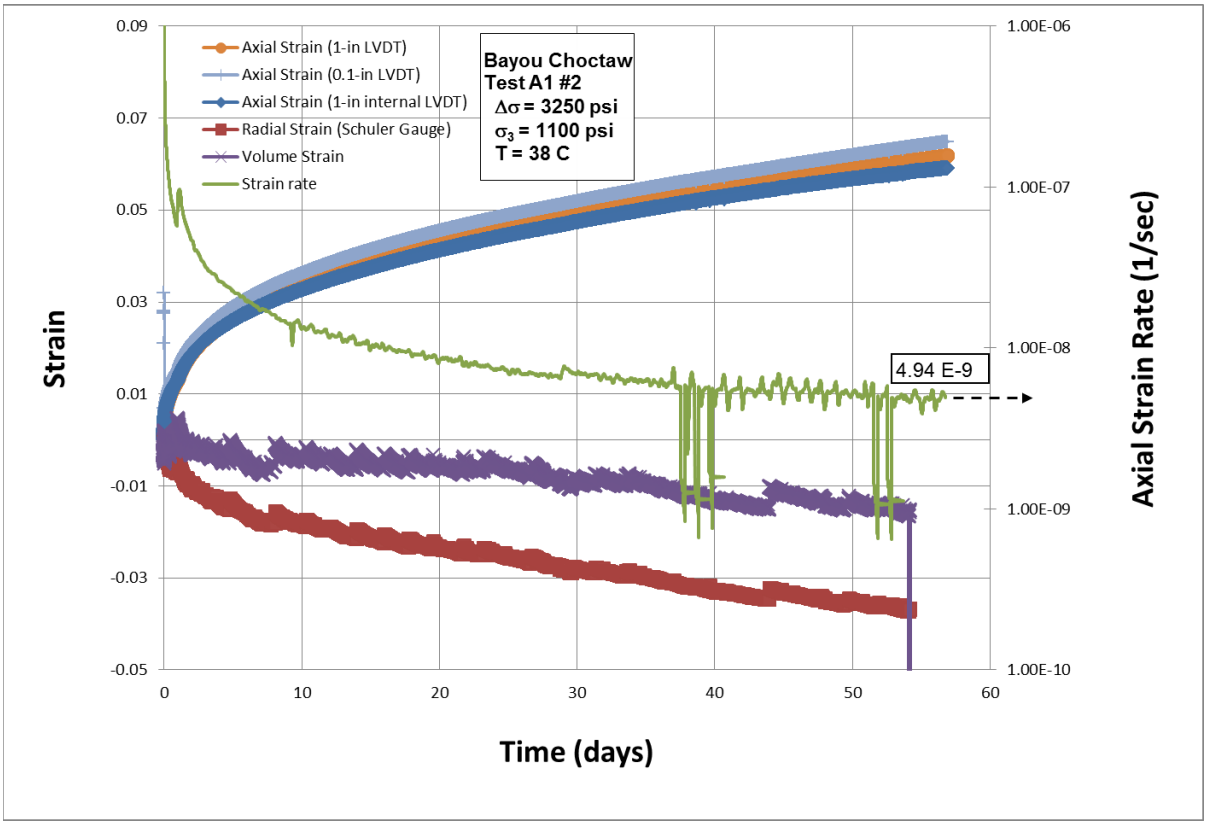

Figure 10. Axial strain, radial strain, and axial strain rate versus time histories for a typical creep test (Test 13) of BC salt, BC-102B.

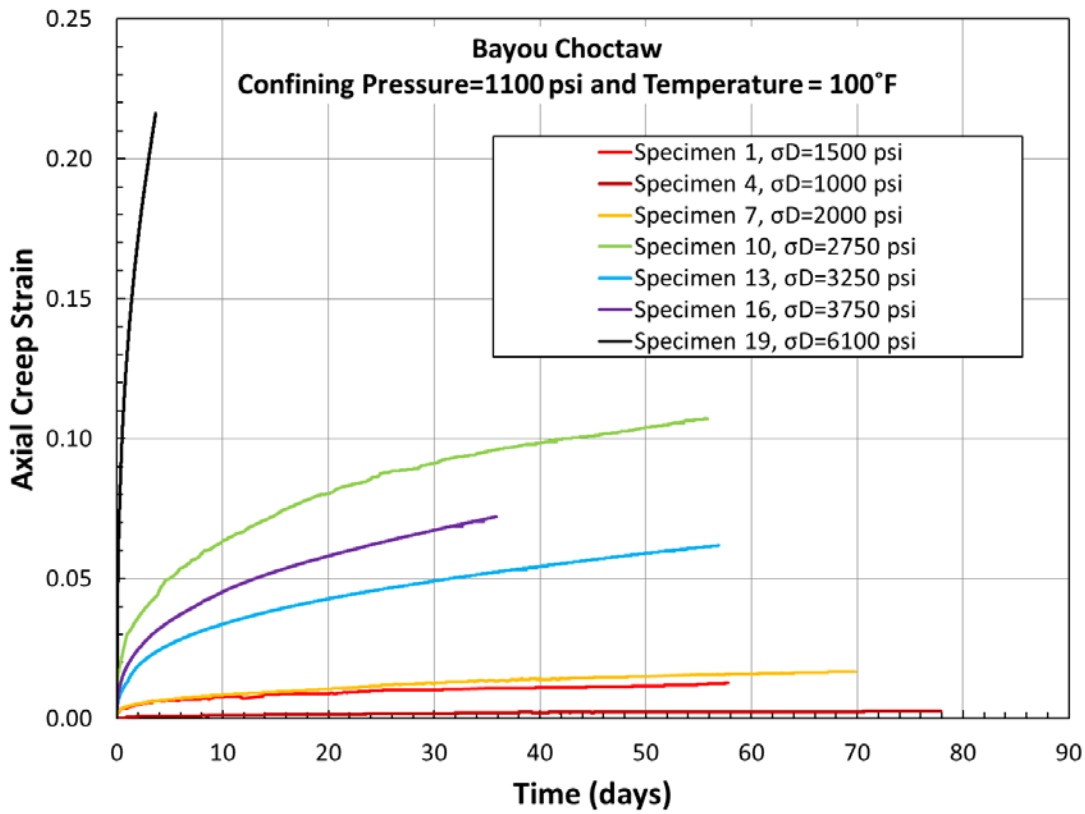

Figure 11. Axial creep strain versus time for all Bayou Choctaw creep tests.

Figure 12: Example of a creep test (Specimen 19) that underwent uniform deformation. (Sample was cut in half parallel to the core axis)

Steady-State Strain Rate Analysis

In this section we discuss creep experiments and derivation of a creep expression for the BC rock salt. Root-mean-square fitting procedures are used in deriving the empirical parameters in the creep expression. The small number of tests performed limits our judgment of the creep expression to an estimate, for example no repeat testing was performed, neither was the effect of temperature or confining pressure investigated.

The creep behavior of salt is often characterized using a steady-state only creep law represented by the following equation:

$$\dot{\varepsilon}_{ss} = A\left(\frac{\Delta\sigma}{\mu}\right)^{n} \exp\left(-\frac{Q}{RT}\right) \qquad \text{Eq 3}$$

where $\dot{\varepsilon}_{ss}$ is the steady-state creep rate, $\Delta\sigma$ is the stress difference, μ is the elastic shear modulus for salt ($\mu = \frac{E}{2(1+\nu)}$), T is temperature (expressed in °K where °K=°C+273), R is the Universal gas constant (1.99 cal/mole°K), and A, n and Q are model parameters. The parameters n and Q are also known as the stress exponent and activation energy, respectively, where the activation energy was assumed to be 10000 cal/mol for this data set [Fossum and Fredrich, 2002]. The model parameters can be determined by fitting Equation 3 to steady-state strain rate data collected at various stress differences and temperatures. Equation 3 can be transformed into linear space by making a few simple assumptions. For example, if all testing is performed at a constant temperature, as the BC test series was, Equation 3 can be re-written as:

$$\dot{\varepsilon}_{ss} = A'\left(\frac{\Delta\sigma}{\mu}\right)^{n} \qquad \text{Eq 4}$$

where A' is a new parameter that incorporates A and the temperature term of Equation 3. Equation 4 can then be linearized through a logarithmic transformation to yield

$$\log(\dot{\varepsilon}_{ss}) = \log(A') + n\log\left(\frac{\Delta\sigma}{\mu}\right) \qquad \text{Eq 5}$$

Plotting steady-state strain rate and stress difference in this transformed space will result in a straight line with a slope of n.

Constant temperature data given in Table 4 (T=100°F) was transformed as defined in Equation 5 and then plotted in the respective transformed space as shown in Figure 13. The data in these plots were fitted using linear-least squares to determine estimates of n. Based on the constant temperatures of 311°K, the value of n was determined to be 4.07. A value of n = 5 is typical of many salts [e.g., Munson et al, 1988].

The value of *n* determined from the linear transformation served as a constant for a nonlinear fitting process used to evaluate the model parameter *A'* in Equation 4 directly. This fitting process made use of the commercially-available **SOLVER** routine included with Microsoft Excel® to yield the following best fit steady-state creep model for BC salt:

$$\dot{\varepsilon}_{ss} = 4.08 \times 10^{10} \left(\frac{\Delta\sigma}{\mu} \right)^{4.07} \qquad \text{Eq 6}$$

All of the steady-state data given in Table 4 was used in the nonlinear fit resulting in the parameter estimate of *A'* shown in Equation 6, this is plotted in Figure 13. Equation 6 was used to predict the steady-state strain rates given in Table 4. These predictions or calculated steady-state rates are shown in Figure 14 and are in good agreement with the measured data.

In Figure 15 the creep expression estimate from this study to that of other rock salts is compared. In order to make a relative comparison, the BC creep data was plotted with the same slope as the other studies shown in Figure 15. To force the BC line to be parallel, the value of n from Equation 4 was set to 5 and A' was allowed to change; the steady state strain rates, shear modulus and stress difference from Equation 4 remained the same. This fitting process again used the SOLVER routine in Excel® to determine an A' value of 7.14 E+13, given an n value of 5. Using n=5 (and Q=10000 cal/mol) is a common assumption in salt rock when an insufficient number of tests have been conducted to completely characterize the salt [Fossum and Fredrich, 2002]. Figure 15 shows the BC rock salt creeps at an intermediate rate compared to other rock salts.

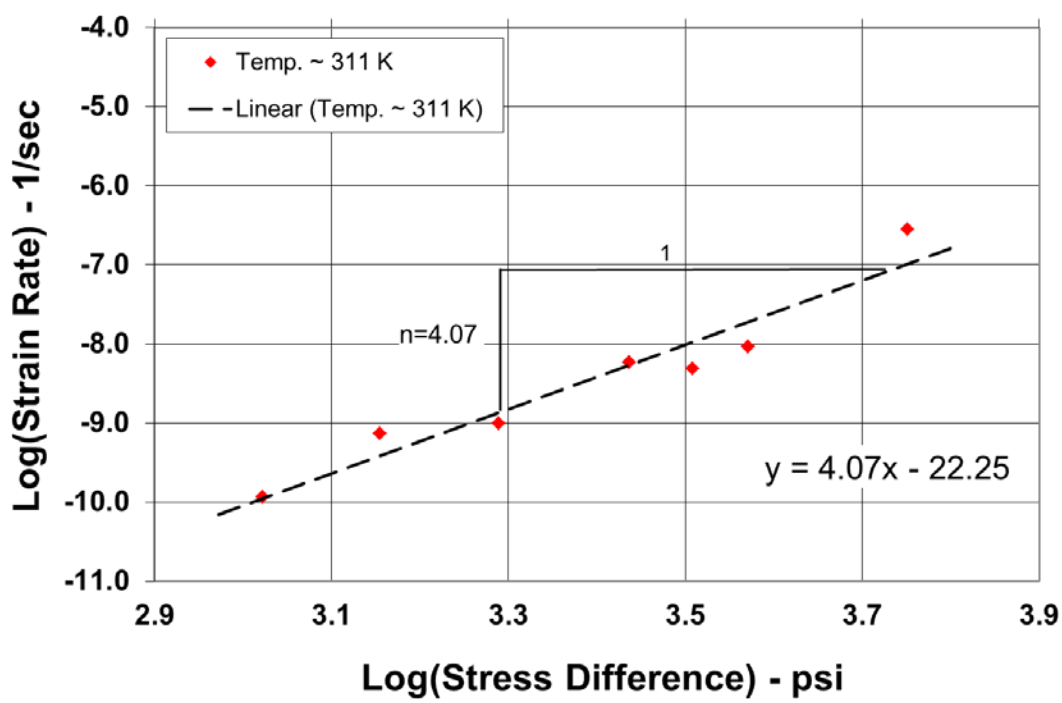

Figure 13. Log steady-state strain rate versus log stress difference for BC salt, BC-102B.

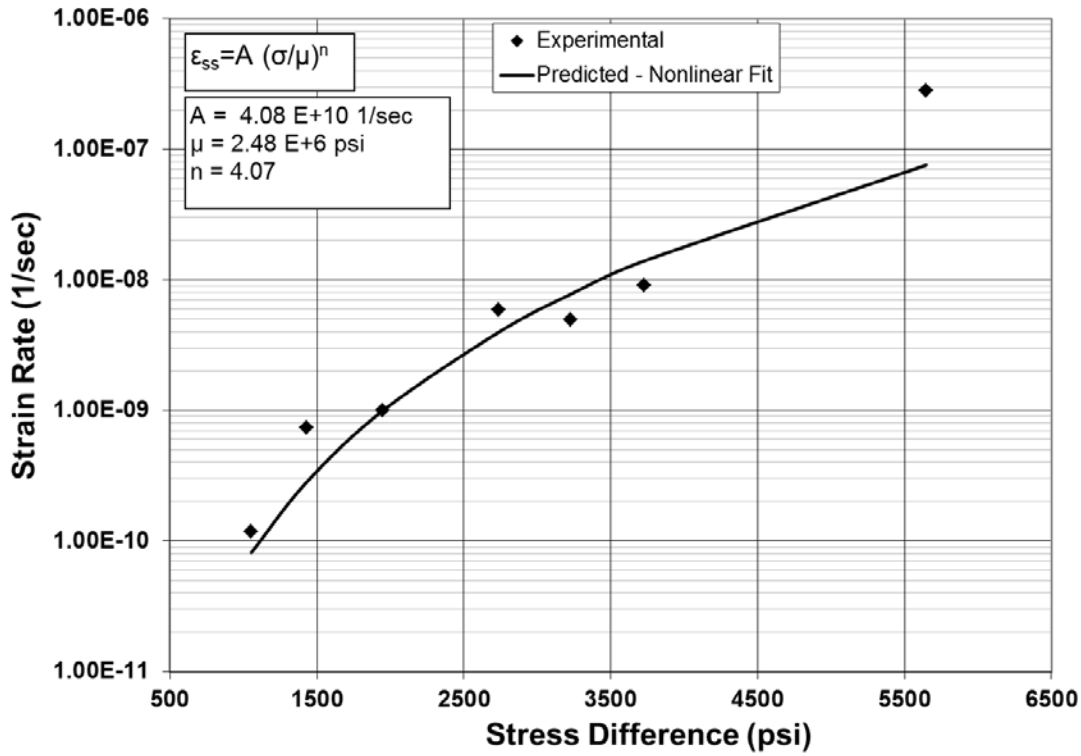

Figure 14. Calculated and measured steady-state strain rates for BC salt, BC-102B.

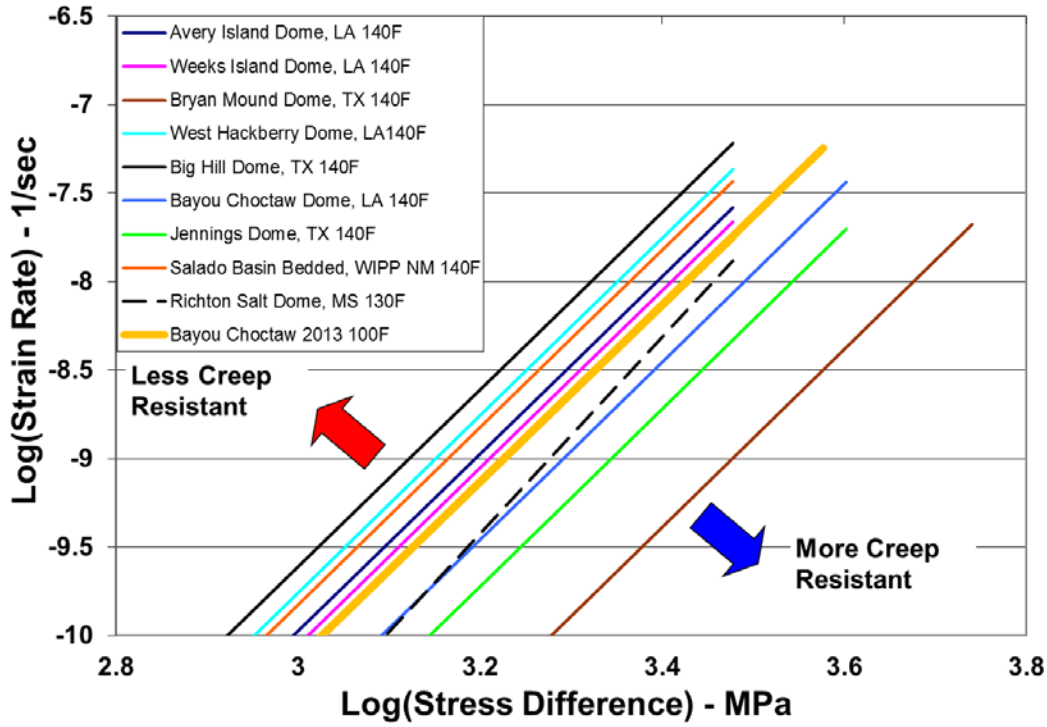

Figure 15. BC creep relation in this study versus that of other Gulf Coast domal salts.

5 Summary and Conclusions

A laboratory testing program was used to examine the mechanical behavior of Bayou Choctaw salt for use in evaluation of a Strategic Petroleum Reserve Bayou Choctaw storage facility. The core was obtained from core hole BC-102B; all comments, inferences, discussions of the BC characterization and analysis are caveated by the small number of tests completed. Mechanical properties testing included: 1) ambient temperature quasi-static axisymmetric compression tests to evaluate dilational stress states and elastic properties; 2) ambient temperature quasi-static axisymmetric extension tests to evaluate dilational stress states and elastic properties; and 3) confined triaxial creep experiments to evaluate the time-dependent behavior of the salt at a constant confining pressure of 1100 psi at 100 $^{\circ}$F.

Twenty one specimens were prepared using this test series; all of which were tested. A small amount of additional core is available for further testing and may be utilized to better refine the properties presented above or to answer new questions should they arise.

It was found that the Young's modulus of the salt ranged from 3.95 x 10^6 to 8.51 x 10^6 psi with an average of 6.44 x 10^6 and generally increased with increasing mean stress (see Table 2). Poisson's ratio ranges from approximately 0.10-0.43 with an average of 0.30. The salt rock density was approximately 2.155 g/cc consistent with visual observational of near pure halite content. The BC dilatational strength criteria determined in this work is defined by the equation $\sqrt{J_2} = 16902 - 16595e^{-.00001039 I_1}$ for the extension tests, and $\sqrt{J_2} = 70575 - 69605e^{-.00000255 I_1}$ for the compression tests.

A steady-state-only creep model has been developed.

$$\dot{\varepsilon}_{ss} = 4.08 \times 10^{10} \left(\frac{\Delta\sigma}{\mu} \right)^{4.07}$$

The creep model suggests that BC rock salt has an intermediate creep resistance when compared to other rock salts in the Strategic Petroleum Reserve, two other other gulf coast domal salts, and bedded salt in the Waste Isolation Pilot Program.

6 Bibliography

ASTM D4543, 1995. Standard Practice for Preparing Rock Core Specimens and Determining Dimensional and Shape Tolerances, American Society for Testing and Materials.

Broome, S. T., S.J. Bauer, D. Dunn, J.H. Hofer, D.R. Bronowski, 2009. Geomechanical Testing of MRIG-9 Core for the Potential SPR Siting at the Richton Salt Dome, SAND2009-0852, Sandia National Laboratories, Albuquerque, New Mexico.

DeVries, K.L., K.D. Mellegard, G.D. Callahan, 2003. Laboratory Testing in Support of a Bedded Salt Failure Criterion, Solution Mining Research Institute Fall Meeting, Chester UK.

Fossum, A.F., J.T. Fredrich, 2002. Salt Mechanics Primer for Near-Salt and Sub Salt Deepwater Gulf of Mexico Field Developments, SAND2002-2063, Sandia National Laboratories, Albuquerque, New Mexico.

Hogan, R. G., 1980, Strategic Petroleum Reserve (SPR) Geological Site Characterization Report Bayou Choctaw Salt Dome, SAND80-7140, Sandia National Laboratories, Albuquerque, New Mexico.

Labuz, J.F., J.M. Bridell, 1993, Reducing frictional constraint in compression testing through lubrication, Int. J. Rock Mech. Min. Sci. 451.

Lee, M.Y., B.L. Ehgartner, and D.R. Bronowski, 2004. Laboratory Evaluation of Damage Criteria and Permeability of Big Hill Salt, SAND2004-6004, Sandia National Laboratories, Albuquerque, NM 87185.

Lord, A.C.S., K.A. Gutierrez, B.L. Roberts, 2013. Bayou Choctaw 102B Salt Core Description (-1065' to -1101'), Internal core condition report, Sandia National Laboratories, Albuquerque, New Mexico.

Mellegard, K. D. and T. W. Pfeifle, 1994. Laboratory Testing of Dome Salt from Weeks Island, Louisiana in Support of the Strategic Petroleum Reserve (SPR) Project, RSI-0552, RE/SPEC Inc., Rapid City, SD.

Munson, D.E., A.F. Fossum, P.E. Senseny, 1988. Advances in Resolution of Discrepancies Between Predicted and Measured In Situ WIPP Room Closures, SAND88-2948, Sandia National Laboratories, Albuquerque, NM.

Neal, J. T., T. R Magorian, K. O. Byrne, and S. Denzler, 1993. Strategic Petroleum Reserve (SPR) Additional Geologic Site Characterization Studies Bayou Choctaw Salt Dome, Louisiana, SAND92-2284, Sandia National Laboratories, Albuquerque, New Mexico 87185, Livermore, California 94550.

Park, B-Y., B.L. Ehgartner, M.Y. Lee, 2006, Three Dimensional Simulation for Bayou Choctaw Strategic Petroleum Reserve (SPR), SAND2006-7589, Sandia National Laboratories, Albuquerque, New Mexico.

Rautman C. A. and J.S. Stein, 2004, Conversion of the Bayou Choctaw Geological Site Characterization Report to a Three-Dimensional Model, SAND2003-3299, Sandia National Laboratories, Albuquerque, NM.

Van Sambeek, L. L, Ratigan, J. L., and F. D. Hansen, 1993. Dilatancy of Rock Salt in Laboratory Tests, Int. J. Rock Mech. Min. Sci. & Geomech. Abstr. Vol. 30, No. 7, pp. 735-738, 1993.

Appendix Summary

Figure A1-1 Stress difference vs. strain for BC salt specimen #3, Mean Stress = 4307 psi, Recovery Depth = 1068.9 ft. 40
Figure A1-2 Stress difference vs. strain for BC salt specimen #6, Mean Stress = 3002 psi, Recovery Depth = 1077.4 ft. 41
Figure A1-3 Stress difference vs. strain for BC salt specimen #9, Mean Stress = 5504 psi, Recovery Depth = 1081.5 ft. 41
Figure A1-4 Stress difference vs. strain for BC salt specimen #12, Mean Stress = 5096 psi, Recovery Depth = 1084.4 ft. 42
Figure A1-5 Stress difference vs. strain for BC salt specimen #15, Mean Stress = 4470 psi, Recovery Depth = 1090.8 ft. This specimen leaked early. 42
Figure A1-6 Stress difference vs. strain for BC salt specimen #18, Mean Stress = 3713 psi, Recovery Depth = 1093.9 ft. 43
Figure A1-7 Stress difference vs. strain for BC salt specimen #21, Mean Stress = 2331 psi, Recovery Depth = 1097.5 ft. This specimen leaked before it could dilate. Note: This graph is plotted on a different scale. 43
Figure A2-1. Stress difference vs. strain for BC salt specimen #2, Mean Stress = 1533 psi, Recovery Depth = 1069.6 ft. 44
Figure A2-2. Stress difference vs. strain for BC salt specimen #5, Mean Stress = 3630 psi, Recovery Depth = 1077.9 ft. 45
Figure A2-3. Stress difference vs. strain for BC salt specimen #8, Mean Stress = 3000 psi, Recovery Depth = 1080.7 ft. 45
Figure A2-4. Stress difference vs. strain for BC salt specimen #11, Mean Stress = 3970 psi, Recovery Depth = 1083.7 ft. 46
Figure A2-5. Stress difference vs. strain for BC salt specimen #14, Mean Stress = 2870 psi, Recovery Depth = 1089.7ft. 46
Figure A2-6. Stress difference vs. strain for BC salt specimen #17, Mean Stress = 2350 psi, Recovery Depth = 1093.2ft. Note: This graph is plotted on a different scale. 47
Figure A2-7. Stress difference vs. strain for BC salt specimen #20, Mean Stress = 2215 psi, Recovery Depth = 1096.6 ft. 47
Figure A3-1a. Creep test #1. Plot of all strains versus time. Confining pressure = 1100 psi, Stress difference = 1500 psi and Temperature = 100°F. Recovery Depth = 1070.2 ft. 48
Figure A3-1b. Creep test #1. Plot of strain rates versus time. Confining pressure = 1100 psi, Stress difference = 1500 psi and Temperature = 100°F. Recovery Depth = 1070.2 ft. The very slow creep tests were performed at the limit of the creep system, as a result the data is noisy. 49
Figure A3-1c. Creep test #1. Plot of stress versus time. Confining pressure = 1100 psi, Stress difference = 1500 psi and Temperature = 100°F. Recovery Depth = 1070.2 ft. 50
Figure A3-1d. Creep test #1. Plot of temperature versus time. Confining pressure = 1100 psi, Stress difference = 1500 psi and Temperature = 100°F. Recovery Depth = 1070.2 ft. 50
Figure A3-2a. Creep test #4. Plot of all strains versus time. Confining pressure = 1100 psi, Stress difference = 1000 psi and Temperature = 100°F. Recovery Depth = 1078.6 ft. The very slow creep tests were performed at the limit of the creep system, as a result the data is noisy. 51
Figure A3-2b. Creep test #4. Plot of strain rates versus time. Confining pressure = 1100 psi, Stress difference = 1000 psi and Temperature = 100°F. Recovery Depth = 1078.6 ft. The very slow creep tests were performed at the limit of the creep system, as a result the data is noisy. 52
Figure A3-2c. Creep test #4. Plot of stress versus time. Confining pressure = 1100 psi, Stress difference = 1000 psi and Temperature = 100°F. Recovery Depth = 1078.6 ft. 53
Figure A3-2d. Creep test #4. Plot of temperature versus time. Confining pressure = 1100 psi, Stress difference = 1000 psi and Temperature = 100°F. Recovery Depth = 1078.6 ft. 53
Figure A3-3a. Creep test #7. Plot of all strains versus time. Confining pressure = 1100 psi, Stress difference = 2000 psi and Temperature = 100°F. Recovery Depth = 1080 ft. 54

Figure A3-3b. Creep test #7. Plot of strain rates versus time. Confining pressure = 1100 psi, Stress difference = 2000 psi and Temperature = 100°F. Recovery Depth = 1080 ft. The slow creep tests were performed at the limit of the creep system, as a result some of the data is noisy. 54
Figure A3-3c. Creep test #7. Plot of stress versus time. Confining pressure = 1100 psi, Stress difference = 2000 psi and Temperature = 100°F. Recovery Depth = 1080 ft. 55
Figure A3-3d. Creep test #7. Plot of temperature versus time. Confining pressure = 1100 psi, Stress difference = 2000 psi and Temperature = 100°F. Recovery Depth = 1080 ft. 55
Figure A3-4a. Creep test #10. Plot of all strains versus time. Confining pressure = 1100 psi, Stress difference = 2750 psi and Temperature = 100°F. Recovery Depth = 1083 ft. The internal LVDTs ran out of range on this specimen, hence the errors with that data. 56
Figure A3-4b. Creep test #10. Plot of strain rates versus time. Confining pressure = 1100 psi, Stress difference = 2750 psi and Temperature = 100°F. Recovery Depth = 1083 ft. The internal LVDTs ran out of range on this specimen, hence the errors with that data. 56
Figure A3-4c. Creep test #10. Plot of stress versus time. Confining pressure = 1100 psi, Stress difference = 2750 psi and Temperature = 100°F. Recovery Depth = 1083 ft. 57
Figure A3-4d. Creep test #10. Plot of temperature versus time. Confining pressure = 1100 psi, Stress difference = 2750 psi and Temperature = 100°F. Recovery Depth = 1083 ft. 57
Figure A3-5a. Creep test #13. Plot of all strains versus time. Confining pressure = 1100 psi, Stress difference = 3250 psi and Temperature = 100°F. Recovery Depth = 1089 ft. Internal LVDTs and the Schuler gage used to measure radial strains were problematic on this specimen. 58
Figure A3-5b. Creep test #13. Plot of strain rates versus time. Confining pressure = 1100 psi, Stress difference = 3250 psi and Temperature = 100°F. Recovery Depth = 1089 ft. Internal LVDTs and the Schuler gage used to measure radial strains were problematic on this specimen. 58
Figure A3-5c. Creep test #13. Plot of stress versus time. Confining pressure = 1100 psi, Stress difference = 3250 psi and Temperature = 100°F. Recovery Depth = 1089 ft. 59
Figure A3-5d. Creep test #13. Plot of temperature versus time. Confining pressure = 1100 psi, Stress difference = 3250 psi and Temperature = 100°F. Recovery Depth = 1089 ft. 59
Figure A3-6a. Creep test #16. Plot of all strains versus time. Confining pressure = 1100 psi, Stress difference = 3750 psi and Temperature = 100°F. Recovery Depth = 1092.5 ft. 60
Figure A3-6b. Creep test #16. Plot of strain rates versus time. Confining pressure = 1100 psi, Stress difference = 3750 psi and Temperature = 100°F. Recovery Depth = 1092.5 ft. 60
Figure A3-6c. Creep test #16. Plot of stress versus time. Confining pressure = 1100 psi, Stress difference = 3750 psi and Temperature = 100°F. Recovery Depth = 1092.5 ft. 61
Figure A3-6d. Creep test #16. Plot of temperature versus time. Confining pressure = 1100 psi, Stress difference = 3750 psi and Temperature = 100°F. Recovery Depth = 1092.5 ft. 61
Figure A3-7a. Creep test #19. Plot of all strains versus time. Confining pressure = 1100 psi, Stress difference = 5850 psi and Temperature = 100°F. Recovery Depth = 1095.9 ft. Due to the high strains in achieved on this specimen, the internal LVDTs and radial Schuler gage both ran out of range. Note: This graph is plotted on a different scale. 62
Figure A3-7b. Creep test #19. Plot of strain rates versus time. Confining pressure = 1100 psi, Stress difference = 5850 psi and Temperature = 100°F. Recovery Depth = 1095.9 ft. Due to the high strains in achieved on this specimen, the internal LVDTs and radial Schuler gage both ran out of range. Note: This graph is plotted on a different scale. 63
Figure A3-7c. Creep test #19. Plot of stress versus time. Confining pressure = 1100 psi, Stress difference = 5850 psi and Temperature = 100°F. Recovery Depth = 1095.9 ft. Note: This graph is plotted on a different scale. 64
Figure A3-7d. Creep test #19. Plot of temperature versus time. Confining pressure = 1100 psi, Stress difference = 5850 psi and Temperature = 100°F. Recovery Depth = 1095.9 ft. Note: This graph is plotted on a different scale. 64

Appendix 1

Axisymmetric Extension Stress-Strain Curves

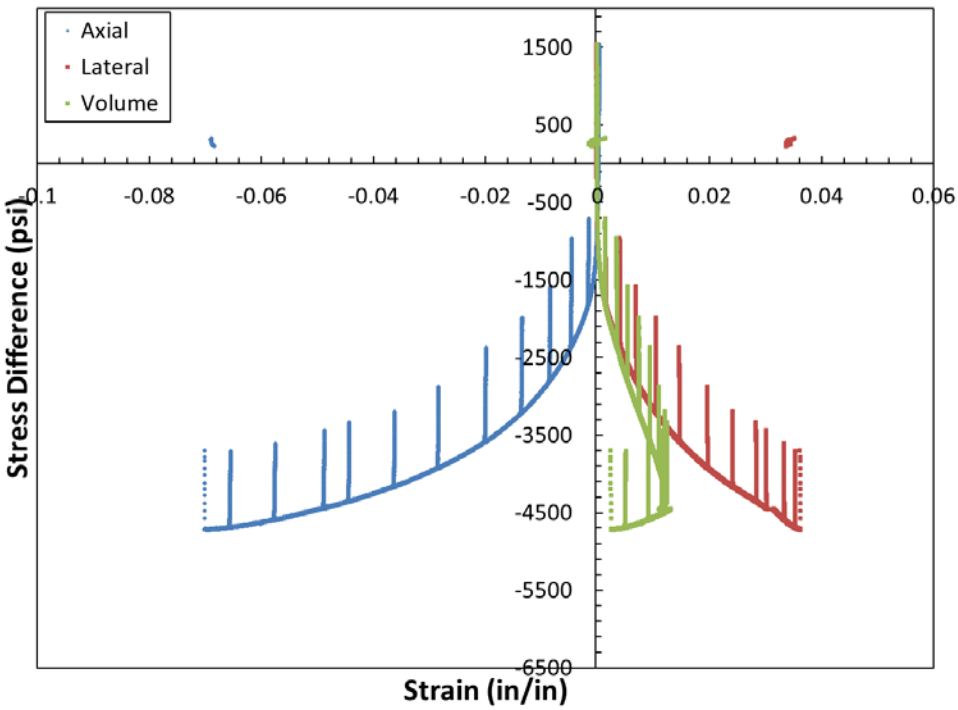

Figure A1-1 Stress difference vs. strain for BC salt specimen #3, Mean Stress = 4307 psi, Recovery Depth = 1068.9 ft.

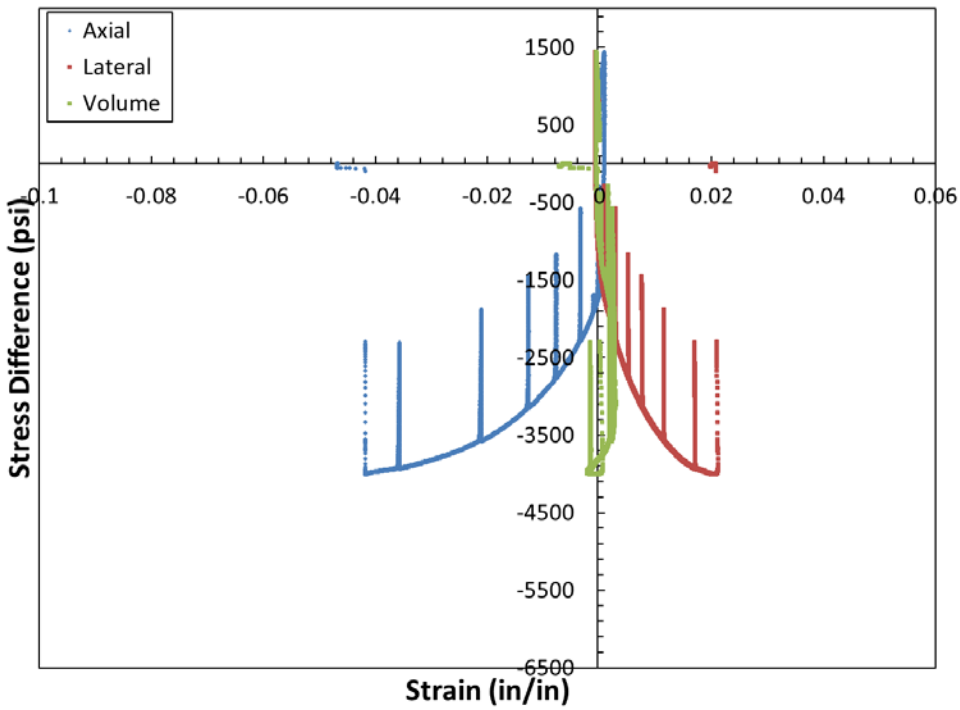

Figure A1-2 Stress difference vs. strain for BC salt specimen #6, Mean Stress = 3002 psi, Recovery Depth = 1077.4 ft.

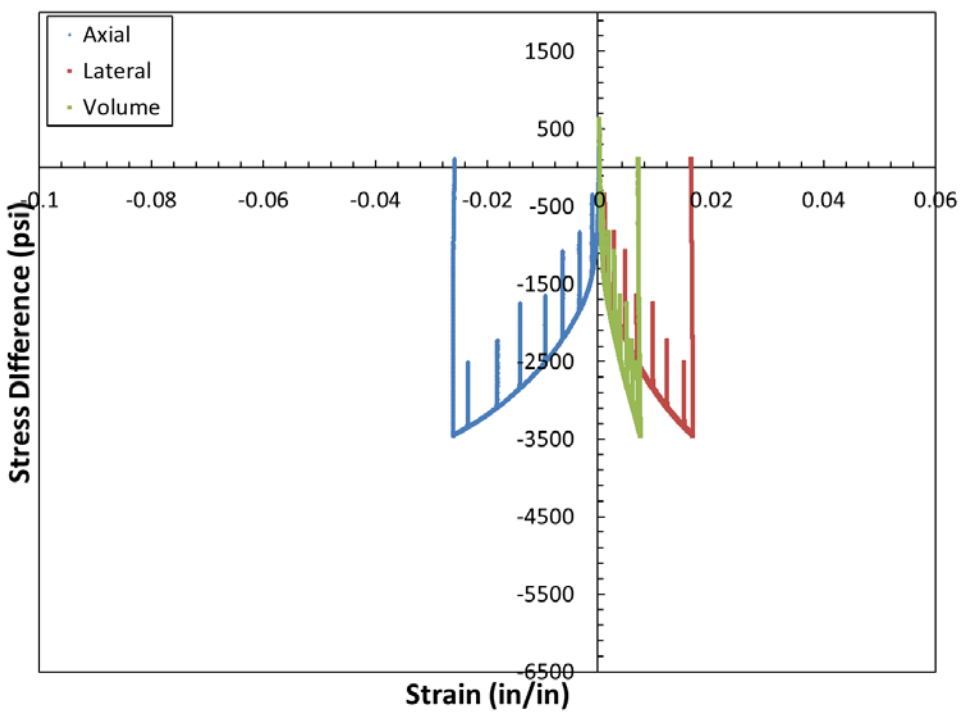

Figure A1-3 Stress difference vs. strain for BC salt specimen #9, Mean Stress = 5504 psi, Recovery Depth = 1081.5 ft.

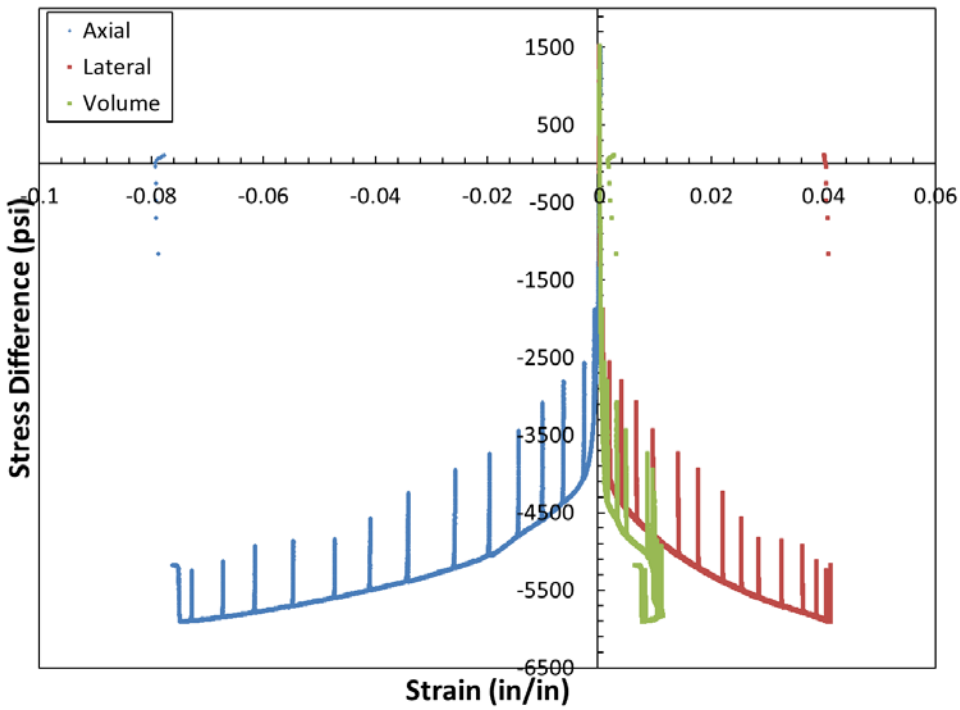

Figure A1-4 Stress difference vs. strain for BC salt specimen #12, Mean Stress = 5096 psi, Recovery Depth = 1084.4 ft.

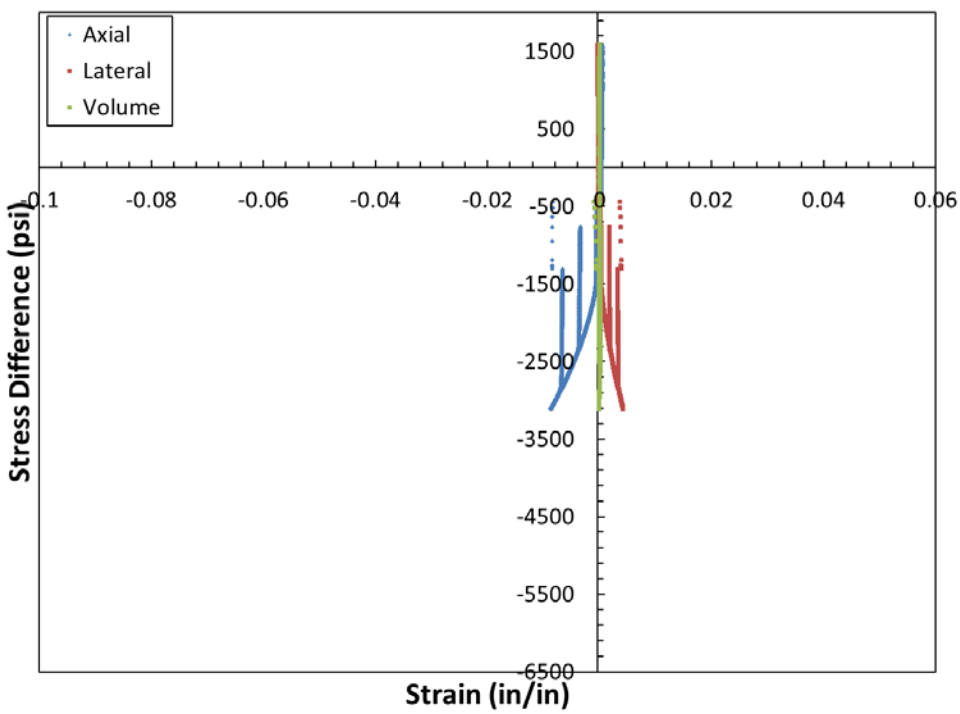

Figure A1-5 Stress difference vs. strain for BC salt specimen #15, Mean Stress = 4470 psi, Recovery Depth = 1090.8 ft. This specimen leaked early.

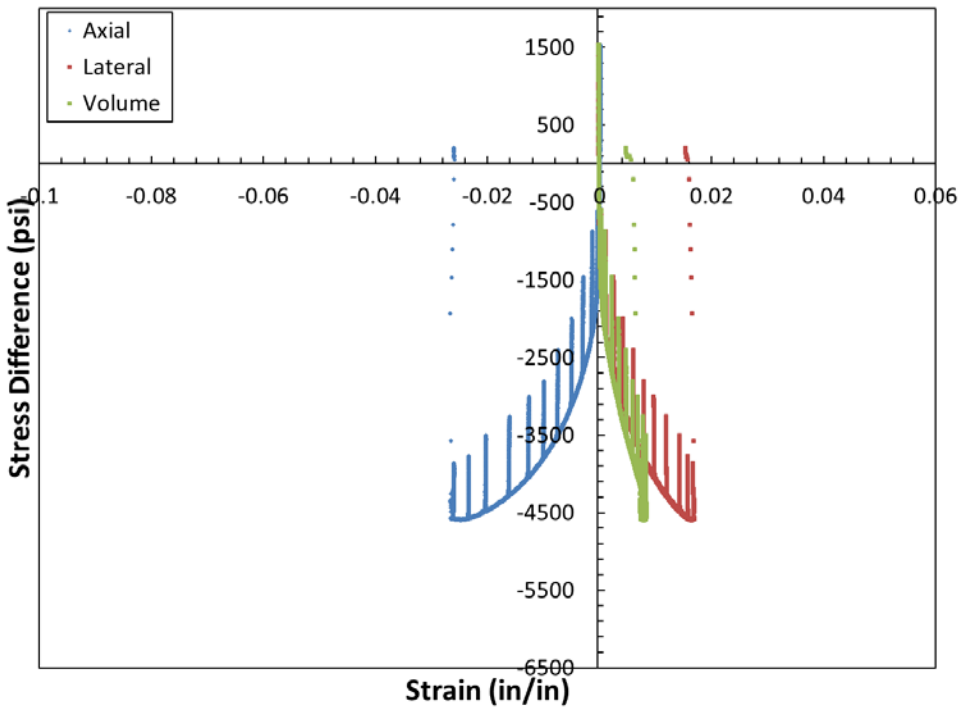

Figure A1-6 Stress difference vs. strain for BC salt specimen #18, Mean Stress = 3713 psi, Recovery Depth = 1093.9 ft.

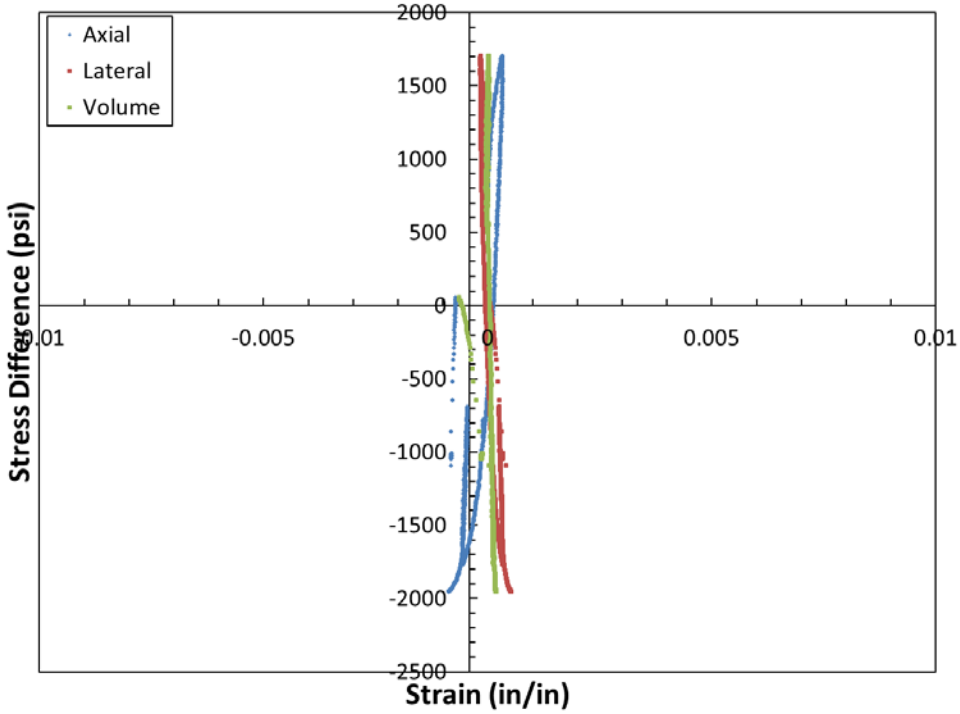

Figure A1-7 Stress difference vs. strain for BC salt specimen #21, Mean Stress = 2331 psi, Recovery Depth = 1097.5 ft. This specimen leaked before it could dilate. Note: This graph is plotted on a different scale.

Appendix 2

Axisymmetric Compression Stress-Strain Curves

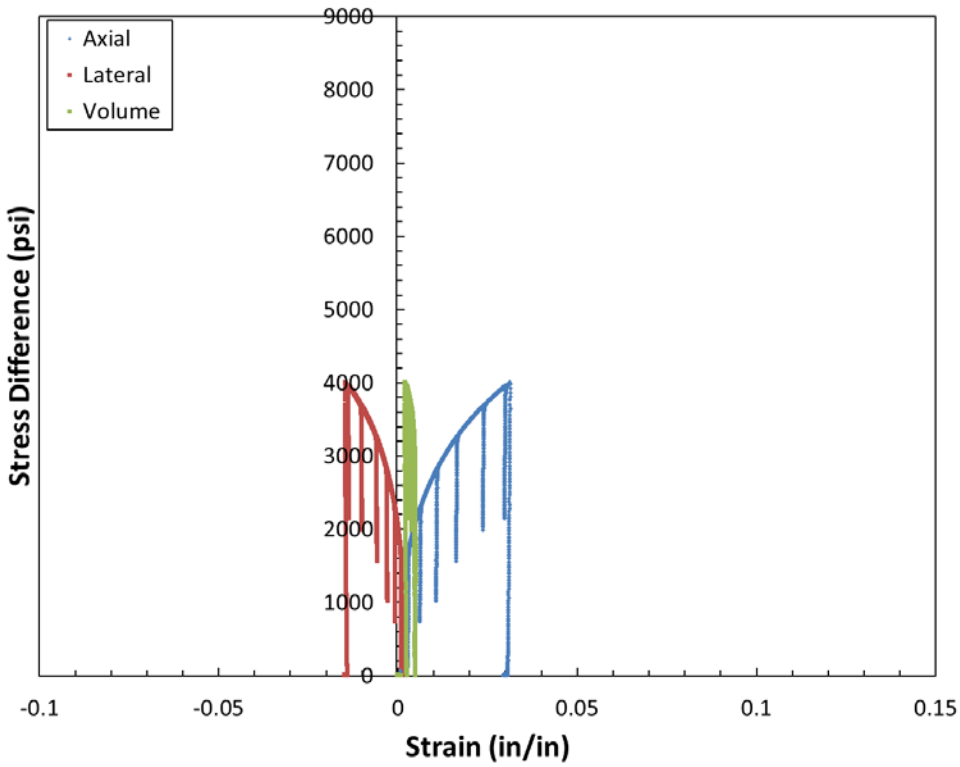

Figure A2-1. Stress difference vs. strain for BC salt specimen #2, Mean Stress = 1533 psi, Recovery Depth = 1069.6 ft.

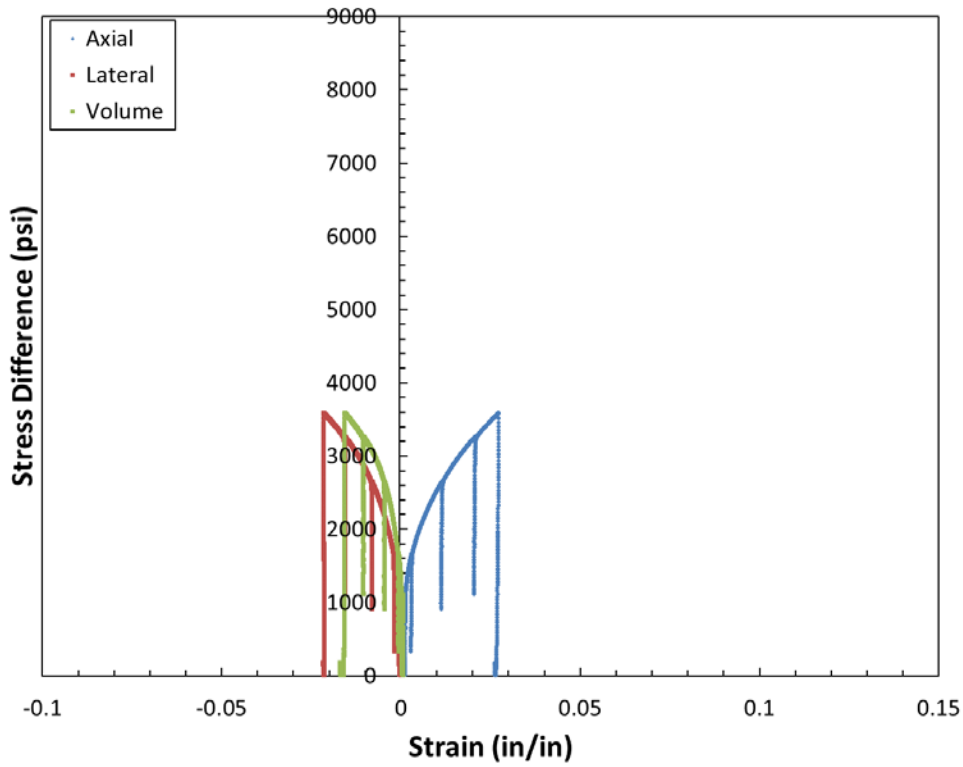

Figure A2-2. Stress difference vs. strain for BC salt specimen #5, Mean Stress = 3630 psi, Recovery Depth = 1077.9 ft.

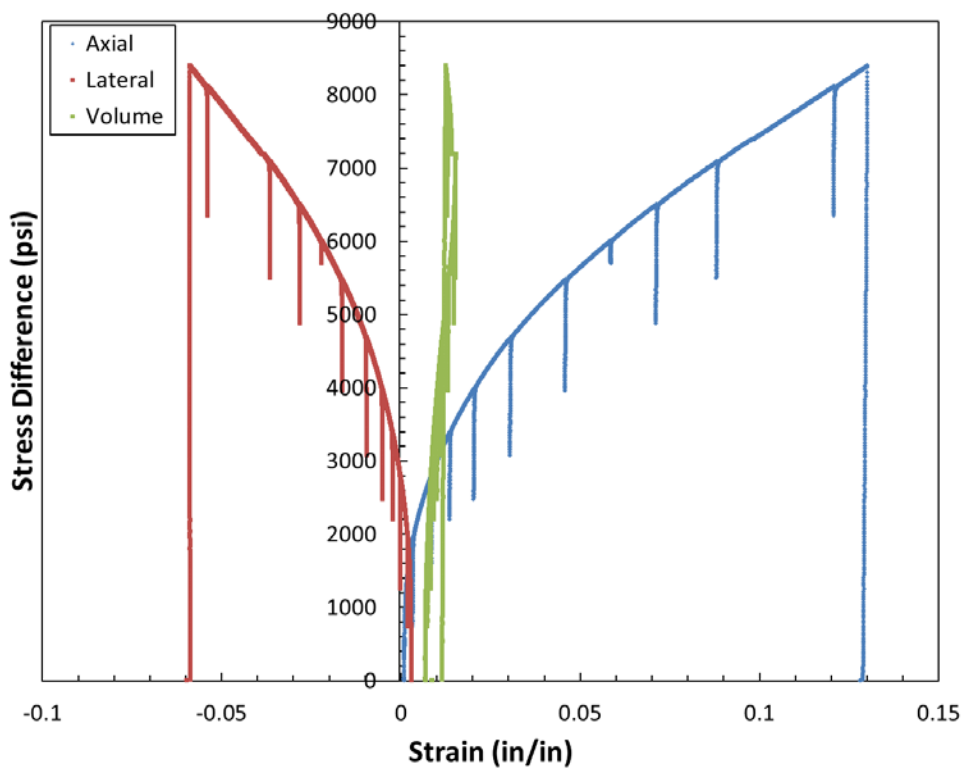

Figure A2-3. Stress difference vs. strain for BC salt specimen #8, Mean Stress = 3000 psi, Recovery Depth = 1080.7 ft.

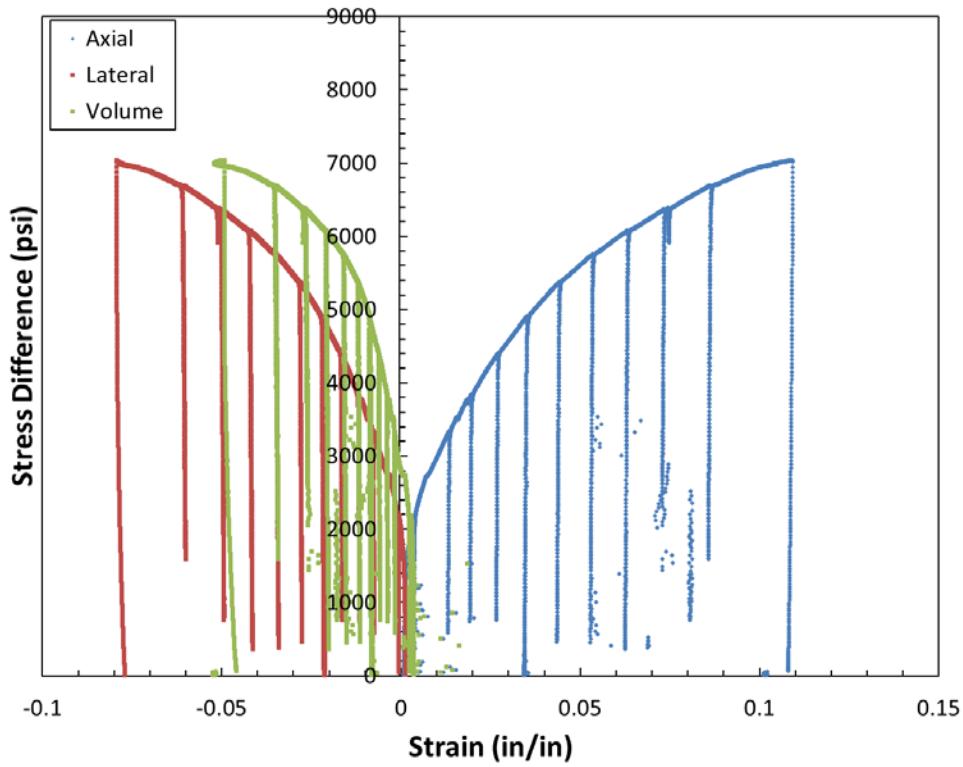

Figure A2-4. Stress difference vs. strain for BC salt specimen #11, Mean Stress = 3970 psi, Recovery Depth = 1083.7 ft.

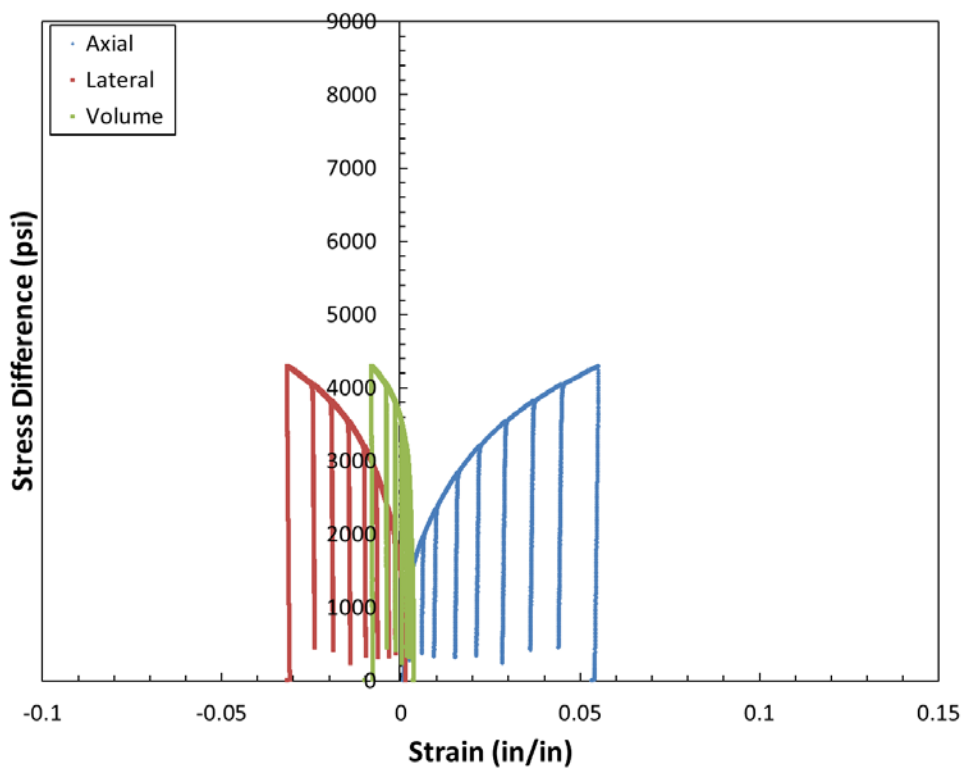

Figure A2-5. Stress difference vs. strain for BC salt specimen #14, Mean Stress = 2870 psi, Recovery Depth = 1089.7ft.

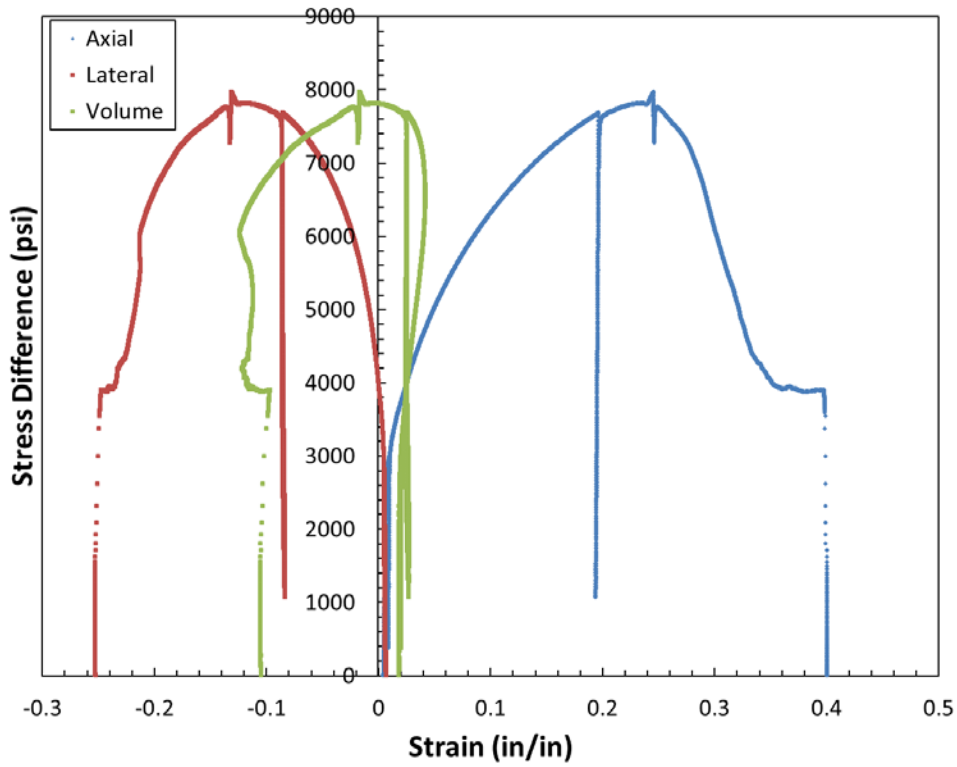

Figure A2-6. Stress difference vs. strain for BC salt specimen #17, Mean Stress = 2350 psi, Recovery Depth = 1093.2ft. Note: This graph is plotted on a different scale.

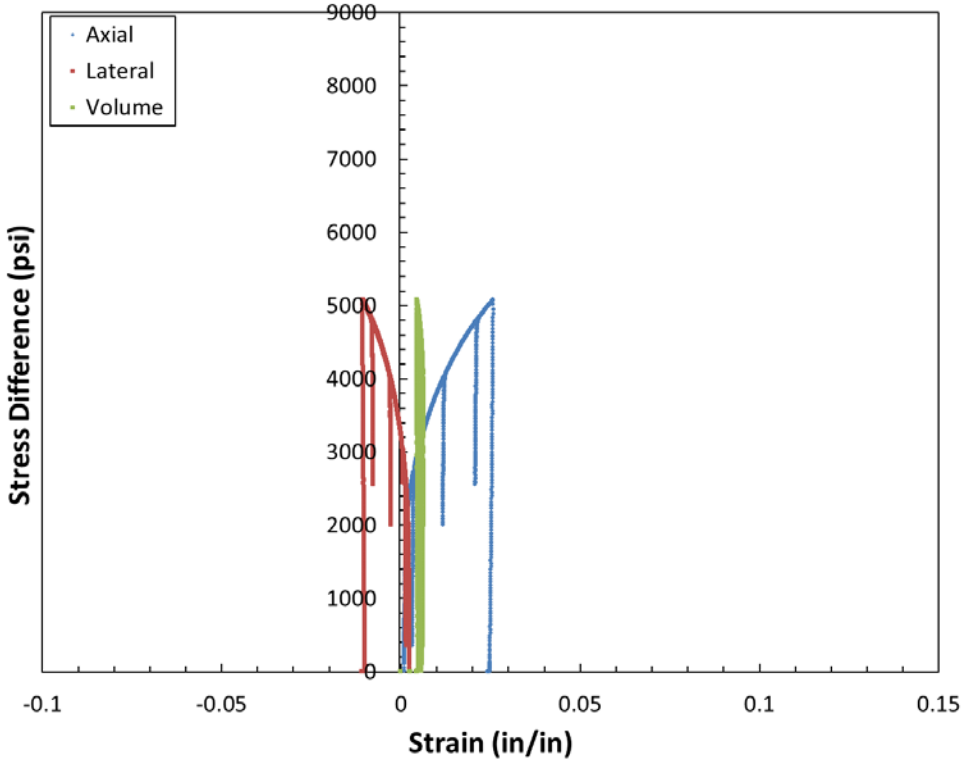

Figure A2-7. Stress difference vs. strain for BC salt specimen #20, Mean Stress = 2215 psi, Recovery Depth = 1096.6 ft.

Appendix 3

Creep tests plots of axial strain, radial strain, volumetric strain, and axial strain rate versus time.

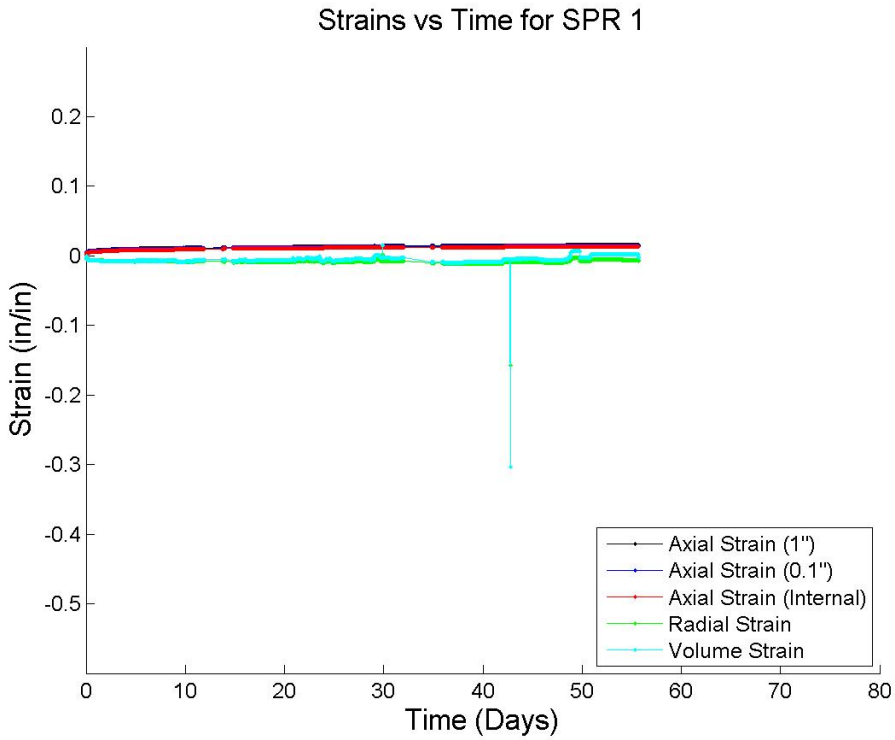

Figure A3-1a. Creep test #1. Plot of all strains versus time. Confining pressure = 1100 psi, Stress difference = 1500 psi and Temperature = 100°F. Recovery Depth = 1070.2 ft.

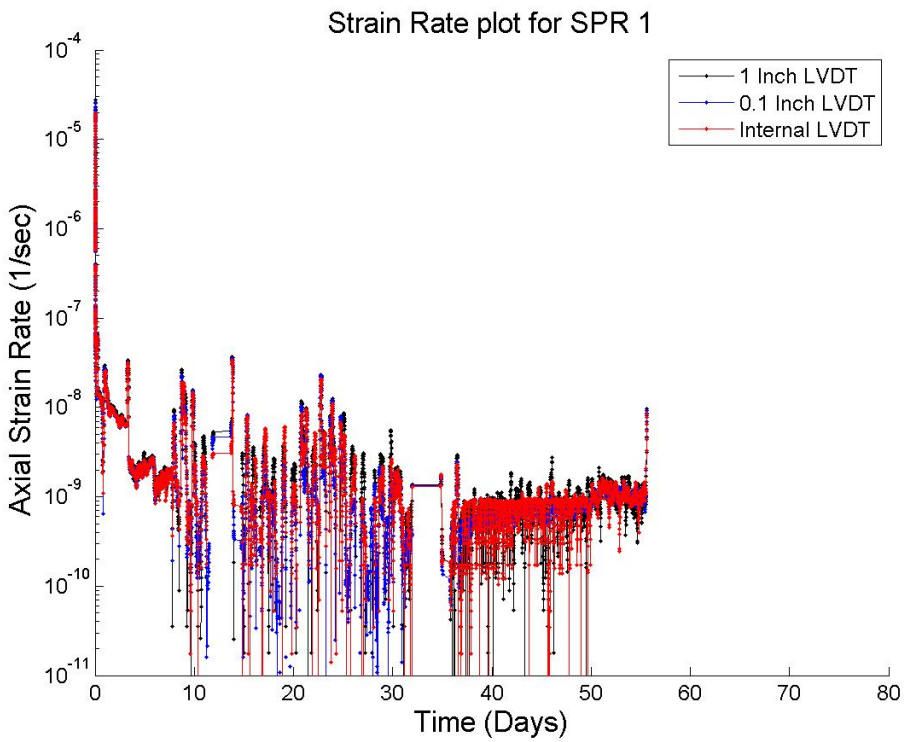

Figure A3-1b. Creep test #1. Plot of strain rates versus time. Confining pressure = 1100 psi, Stress difference = 1500 psi and Temperature = 100°F. Recovery Depth = 1070.2 ft. The very slow creep tests were performed at the limit of the creep system, as a result the data is noisy.

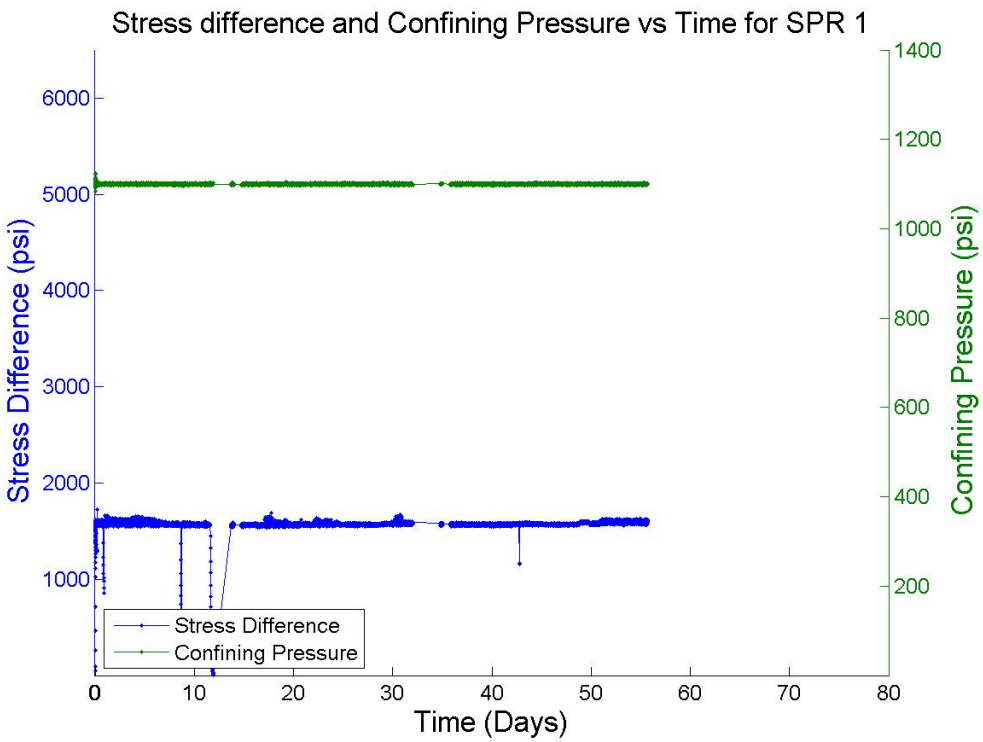

Figure A3-1c. Creep test #1. Plot of stress versus time. Confining pressure = 1100 psi, Stress difference = 1500 psi and Temperature = 100°F. Recovery Depth = 1070.2 ft.

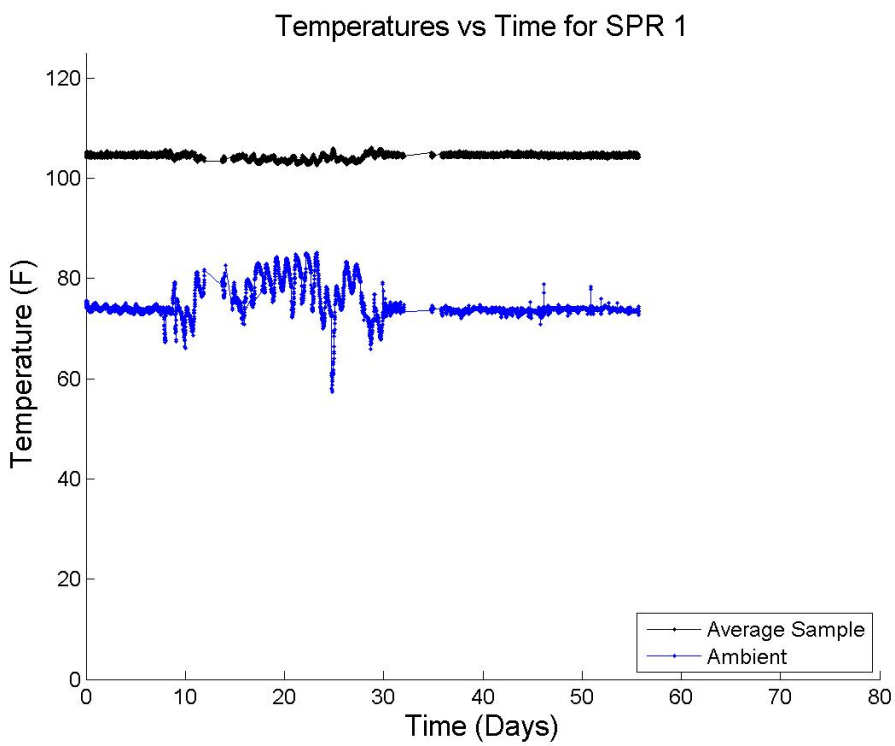

Figure A3-1d. Creep test #1. Plot of temperature versus time. Confining pressure = 1100 psi, Stress difference = 1500 psi and Temperature = 100°F. Recovery Depth = 1070.2 ft.

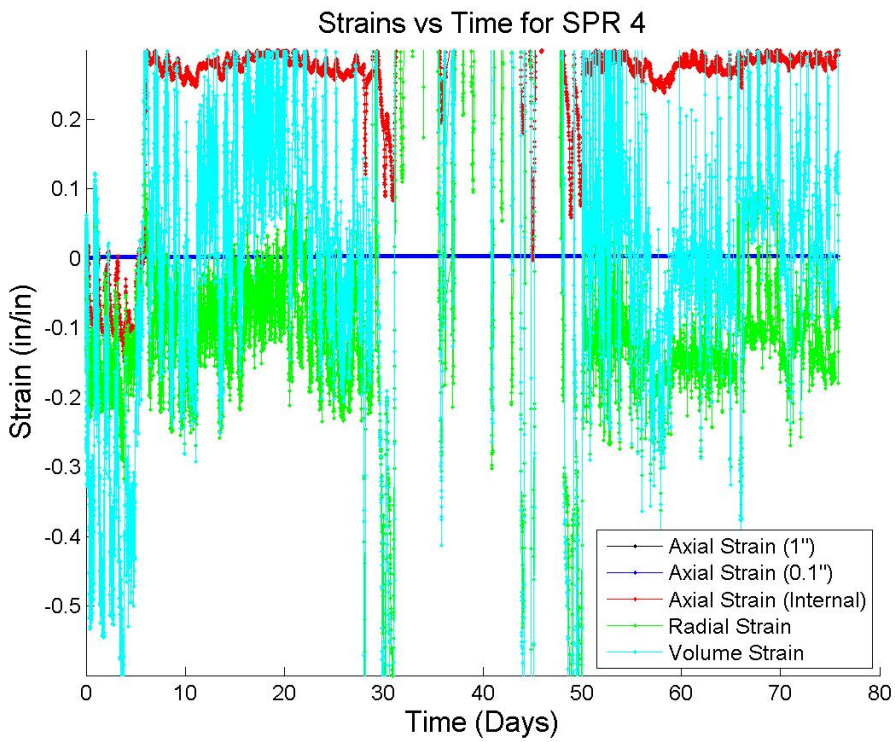

Figure A3-2a. Creep test #4. Plot of all strains versus time. Confining pressure = 1100 psi, Stress difference = 1000 psi and Temperature = 100°F. Recovery Depth = 1078.6 ft. The very slow creep tests were performed at the limit of the creep system, as a result the data is noisy.

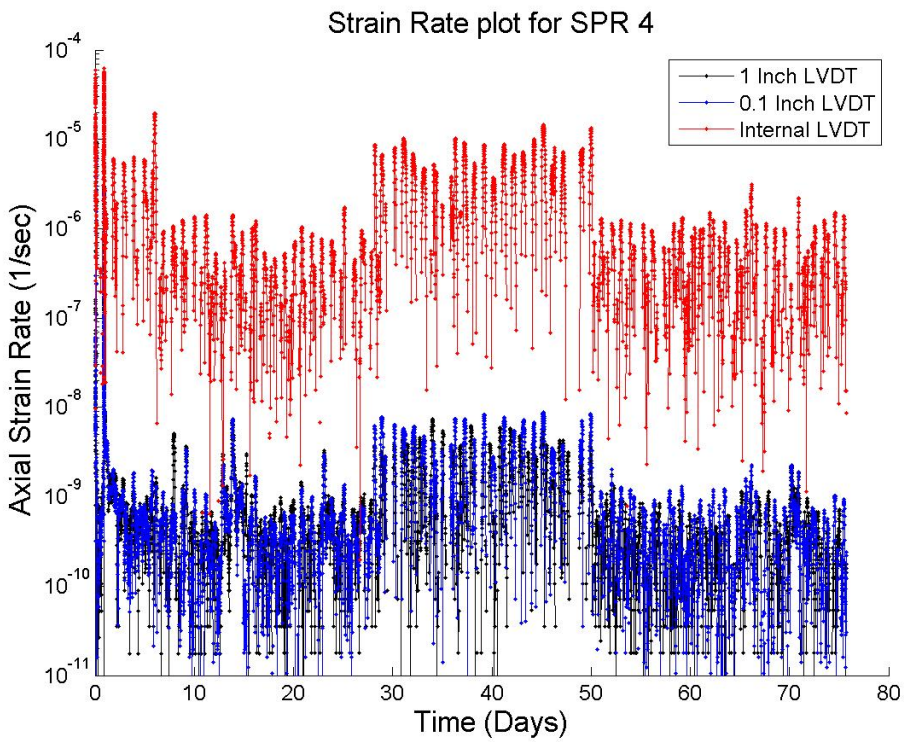

Figure A3-2b. Creep test #4. Plot of strain rates versus time. Confining pressure = 1100 psi, Stress difference = 1000 psi and Temperature = 100°F. Recovery Depth = 1078.6 ft. The very slow creep tests were performed at the limit of the creep system, as a result the data is noisy.

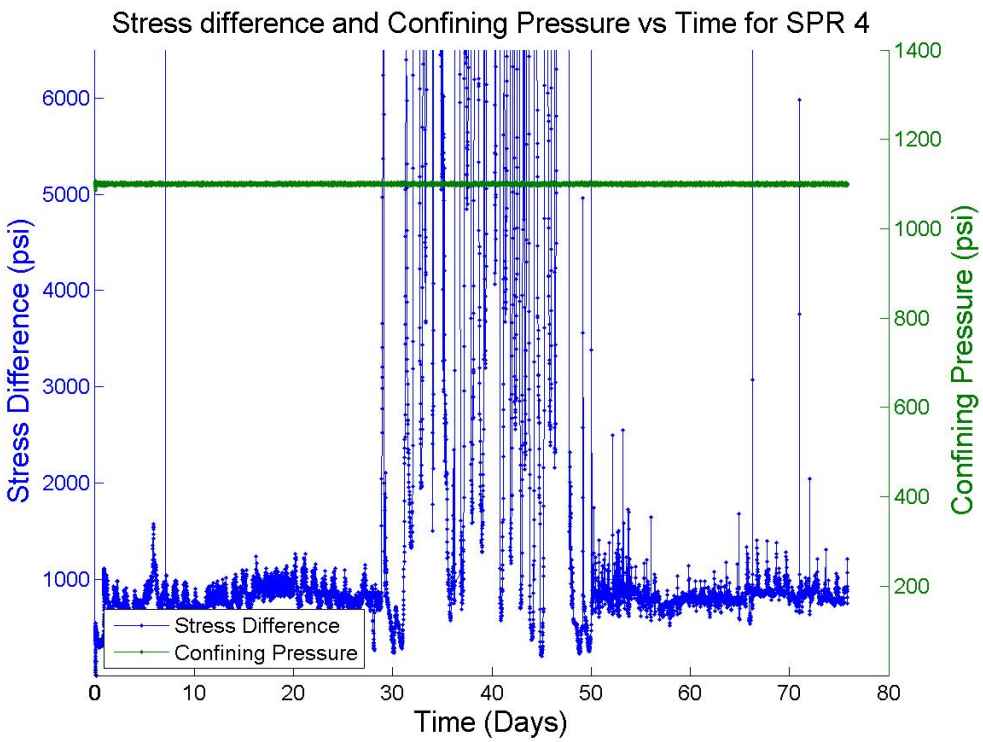

Figure A3-2c. Creep test #4. Plot of stress versus time. Confining pressure = 1100 psi, Stress difference = 1000 psi and Temperature = 100°F. Recovery Depth = 1078.6 ft.

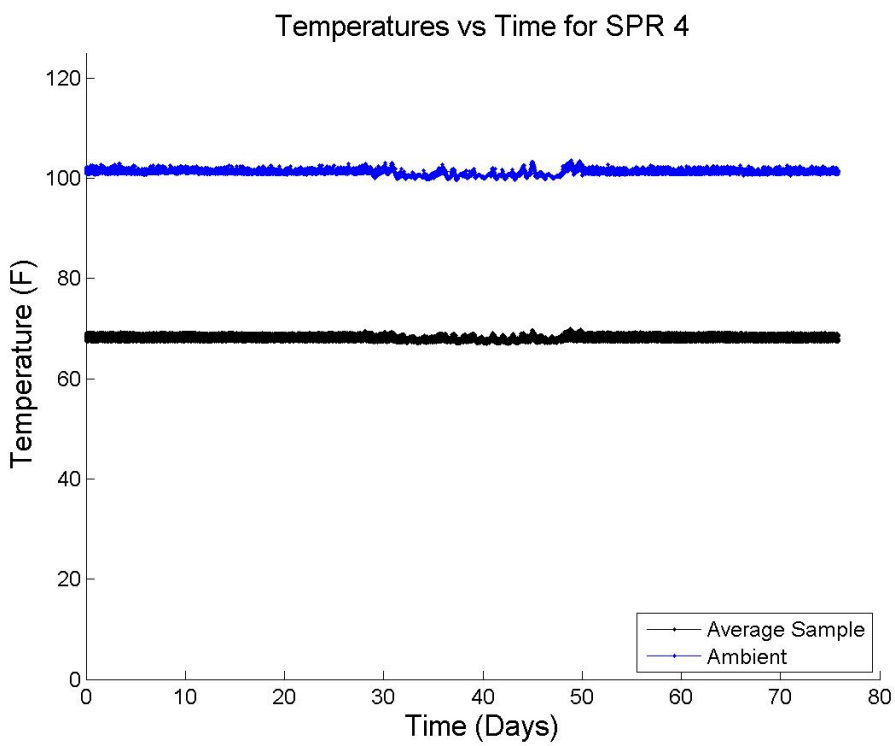

Figure A3-2d. Creep test #4. Plot of temperature versus time. Confining pressure = 1100 psi, Stress difference = 1000 psi and Temperature = 100°F. Recovery Depth = 1078.6 ft.

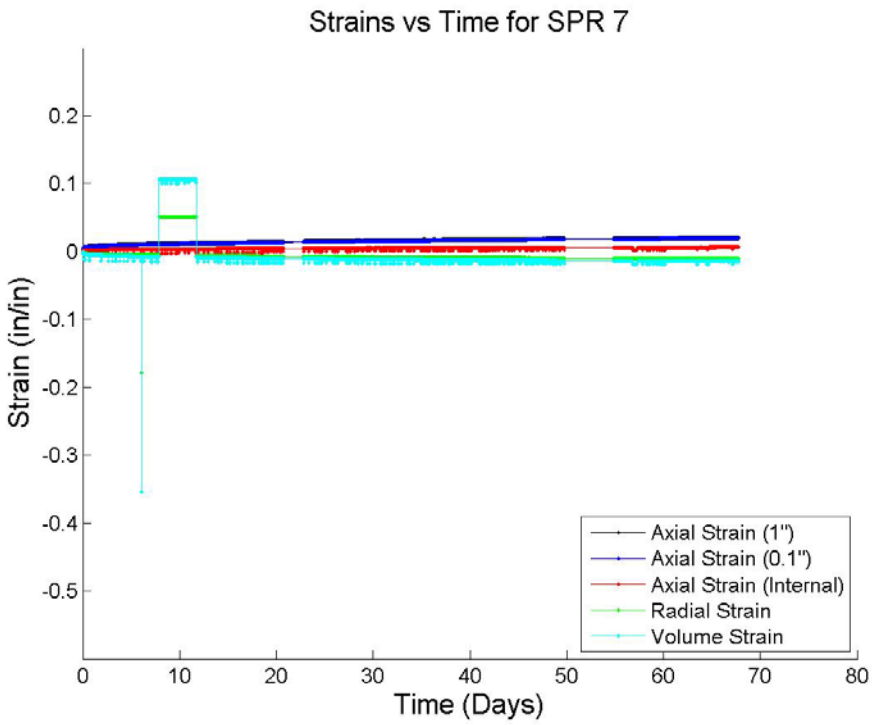

Figure A3-3a. Creep test #7. Plot of all strains versus time. Confining pressure = 1100 psi, Stress difference = 2000 psi and Temperature = 100°F. Recovery Depth = 1080 ft.

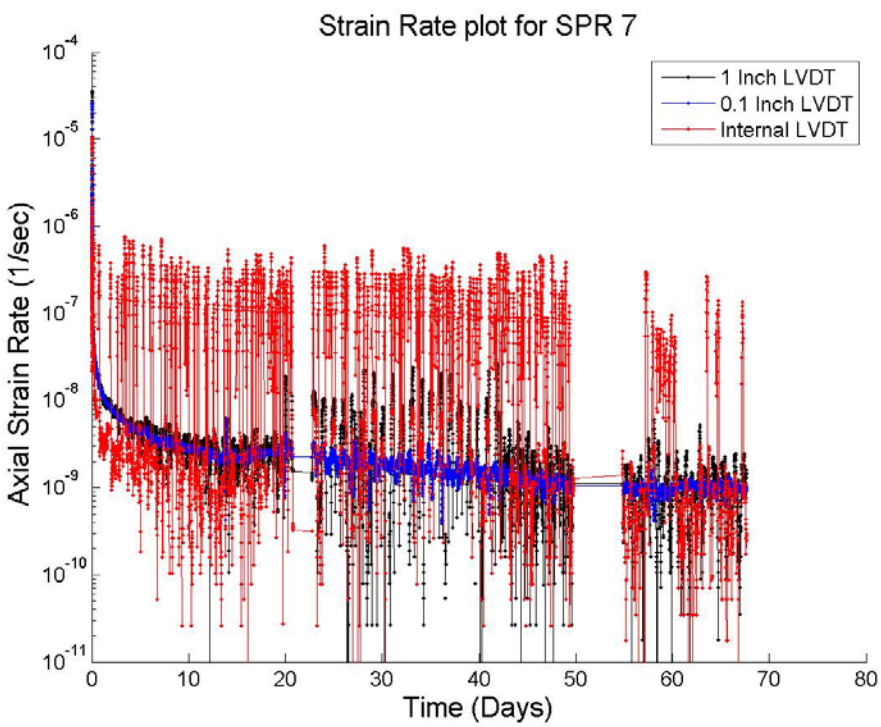

Figure A3-3b. Creep test #7. Plot of strain rates versus time. Confining pressure = 1100 psi, Stress difference = 2000 psi and Temperature = 100°F. Recovery Depth = 1080 ft. The slow creep tests were performed at the limit of the creep system, as a result some of the data is noisy.

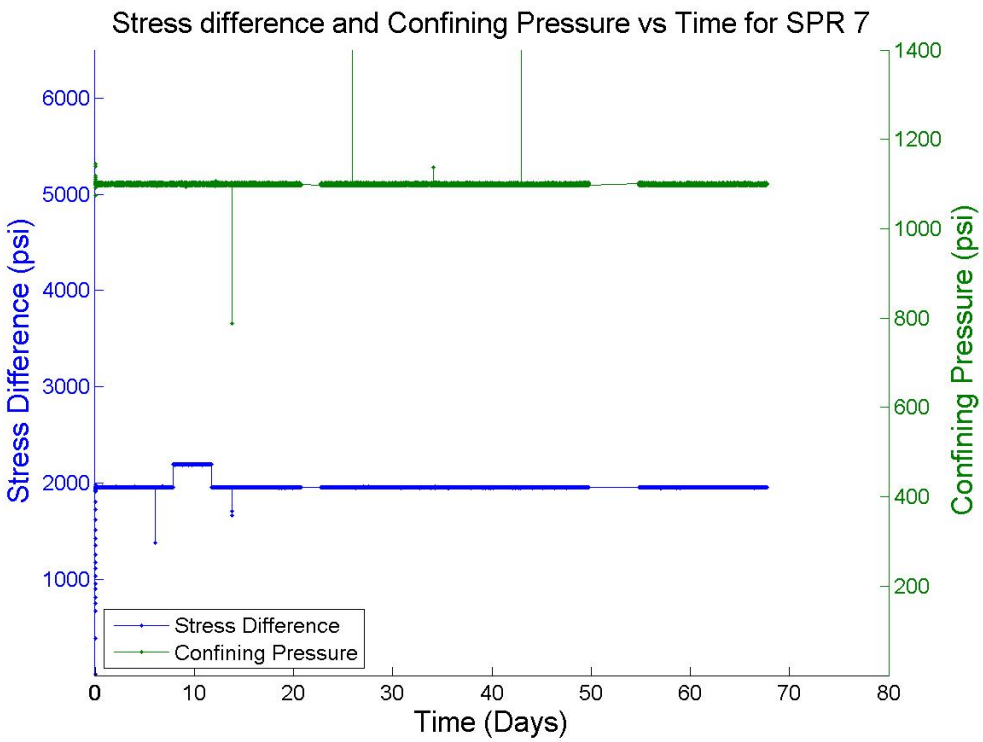

Figure A3-3c. Creep test #7. Plot of stress versus time. Confining pressure = 1100 psi, Stress difference = 2000 psi and Temperature = 100°F. Recovery Depth = 1080 ft.

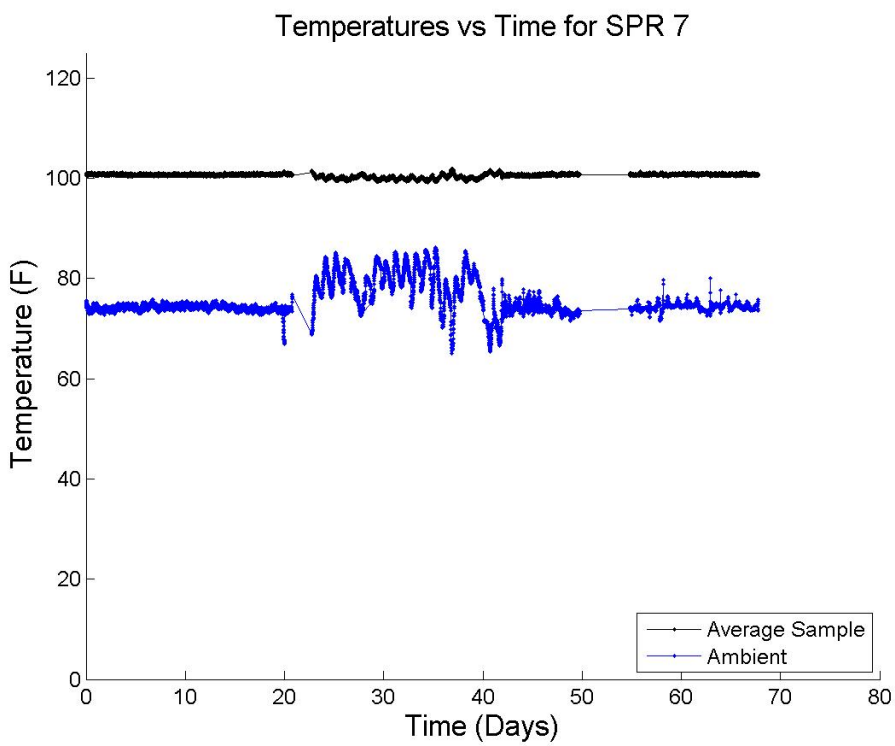

Figure A3-3d. Creep test #7. Plot of temperature versus time. Confining pressure = 1100 psi, Stress difference = 2000 psi and Temperature = 100°F. Recovery Depth = 1080 ft.

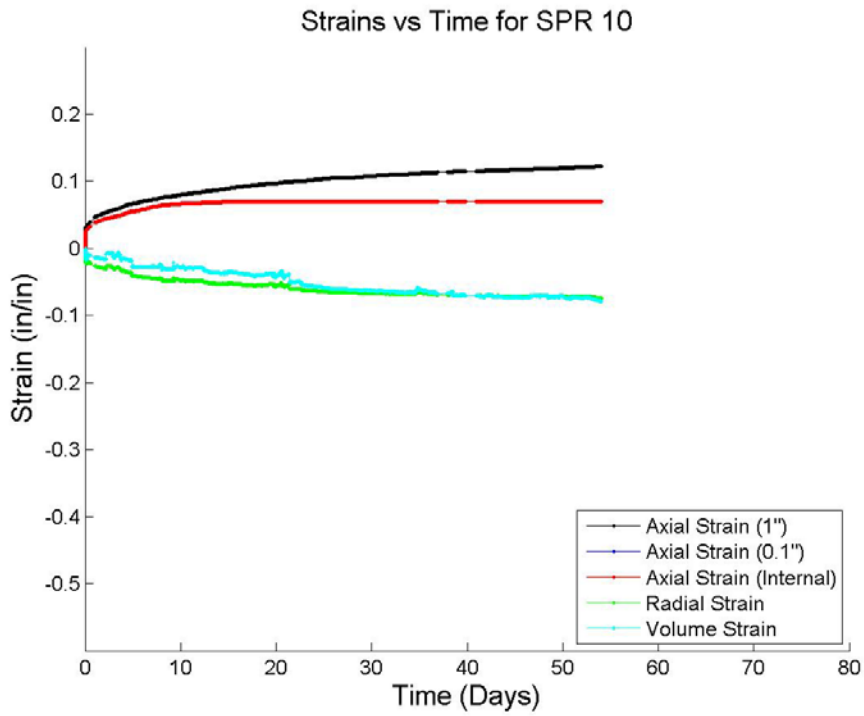

Figure A3-4a. Creep test #10. Plot of all strains versus time. Confining pressure = 1100 psi, Stress difference = 2750 psi and Temperature = 100°F. Recovery Depth = 1083 ft. The internal LVDTs ran out of range on this specimen, hence the errors with that data.

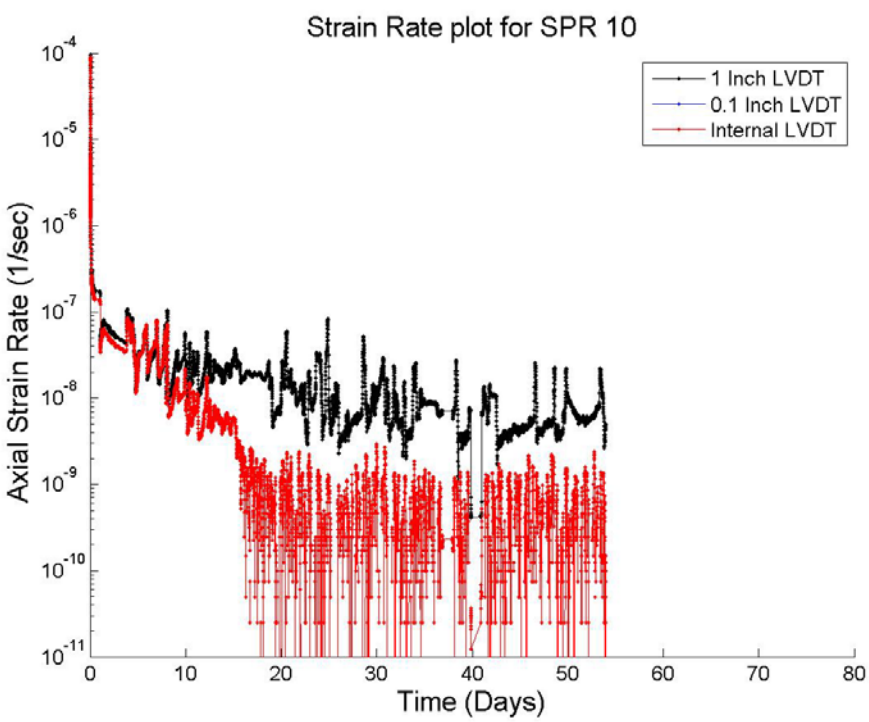

Figure A3-4b. Creep test #10. Plot of strain rates versus time. Confining pressure = 1100 psi, Stress difference = 2750 psi and Temperature = 100°F. Recovery Depth = 1083 ft. The internal LVDTs ran out of range on this specimen, hence the errors with that data.

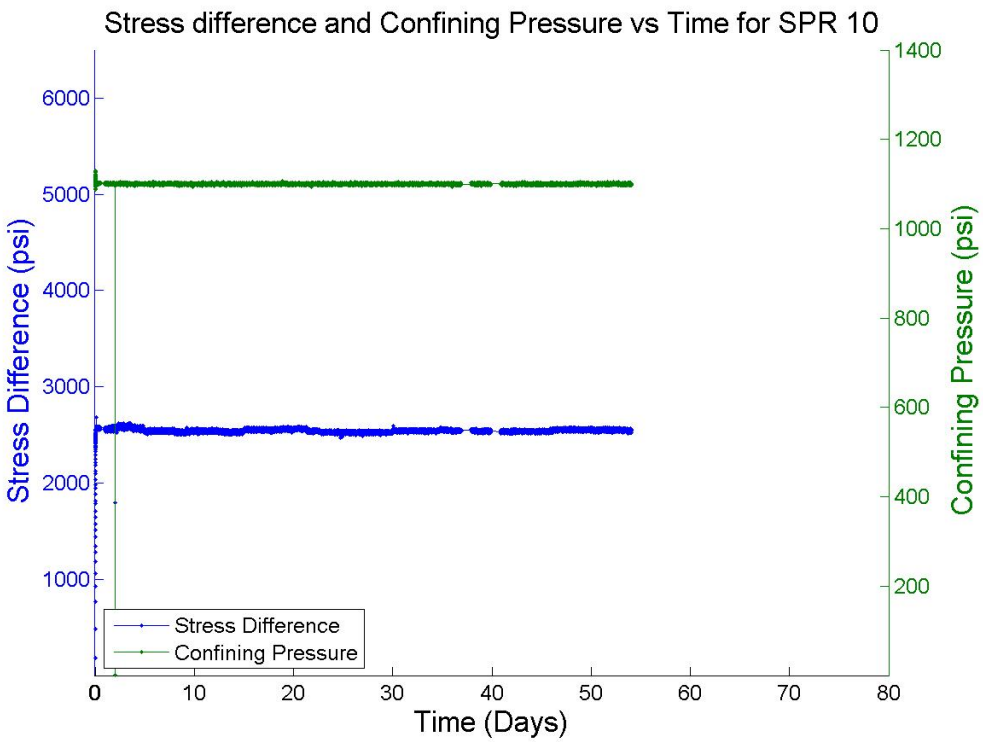

Figure A3-4c. Creep test #10. Plot of stress versus time. Confining pressure = 1100 psi, Stress difference = 2750 psi and Temperature = 100°F. Recovery Depth = 1083 ft.

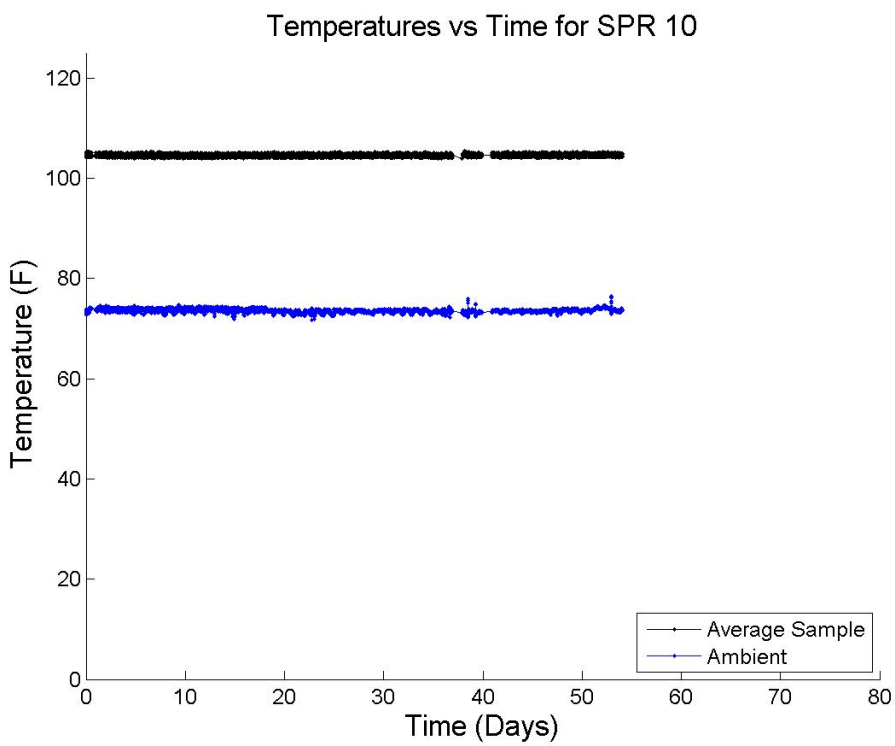

Figure A3-4d. Creep test #10. Plot of temperature versus time. Confining pressure = 1100 psi, Stress difference = 2750 psi and Temperature = 100°F. Recovery Depth = 1083 ft.

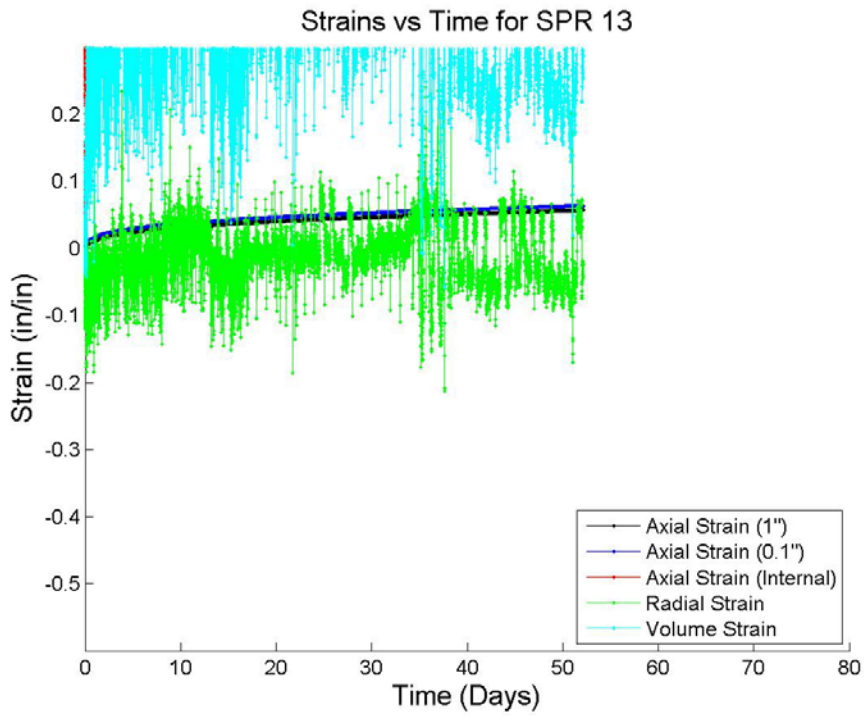

Figure A3-5a. Creep test #13. Plot of all strains versus time. Confining pressure = 1100 psi, Stress difference = 3250 psi and Temperature = 100°F. Recovery Depth = 1089 ft. Internal LVDTs and the Schuler gage used to measure radial strains were problematic on this specimen.

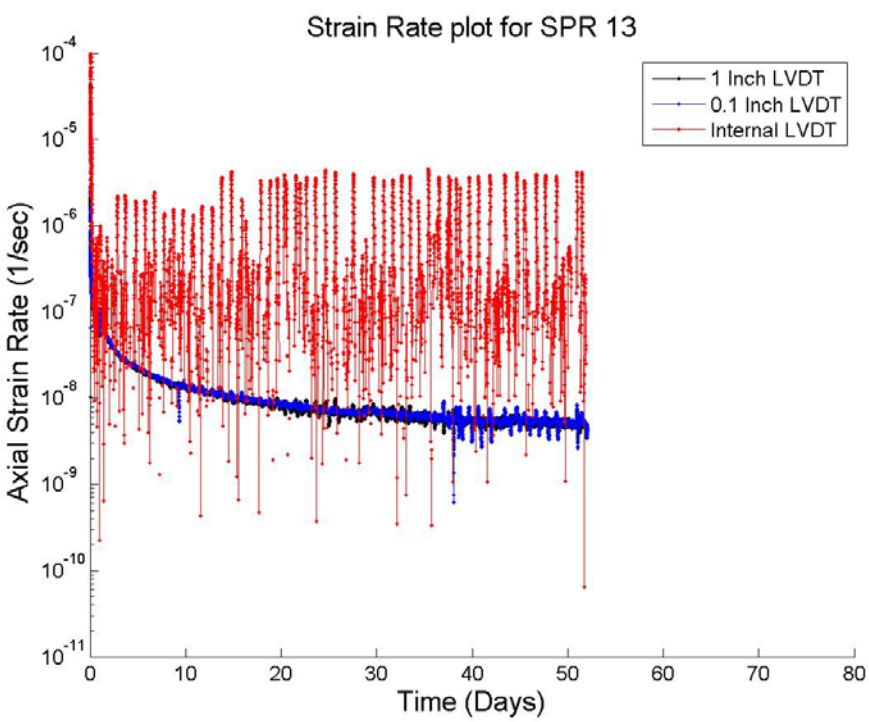

Figure A3-5b. Creep test #13. Plot of strain rates versus time. Confining pressure = 1100 psi, Stress difference = 3250 psi and Temperature = 100°F. Recovery Depth = 1089 ft. Internal LVDTs and the Schuler gage used to measure radial strains were problematic on this specimen.

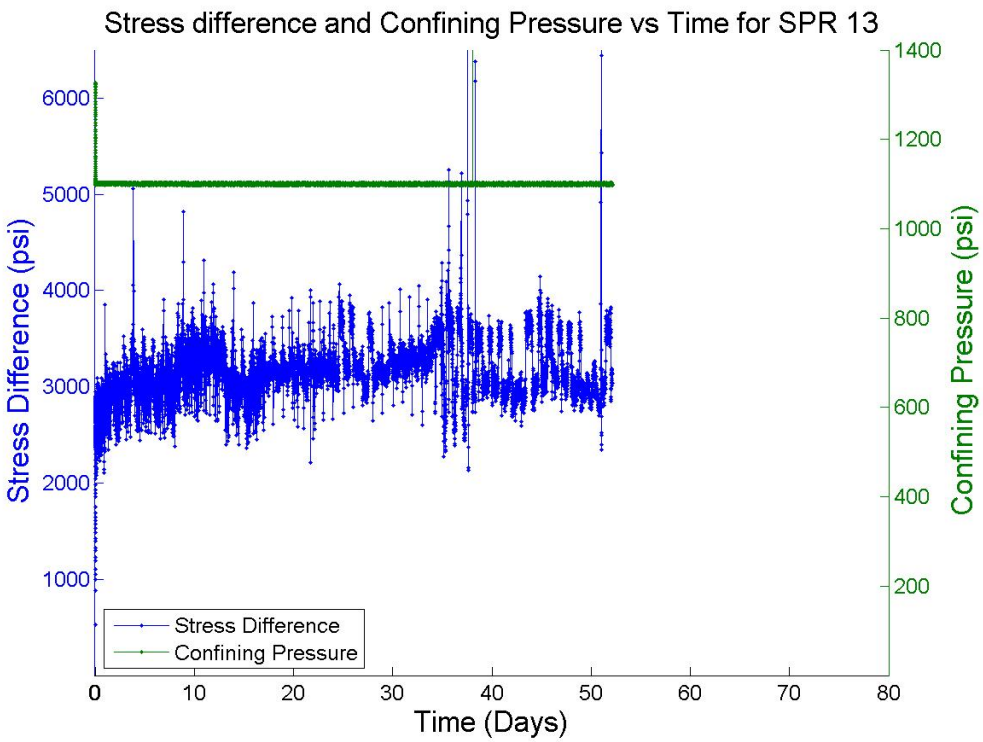

Figure A3-5c. Creep test #13. Plot of stress versus time. Confining pressure = 1100 psi, Stress difference = 3250 psi and Temperature = 100°F. Recovery Depth = 1089 ft.

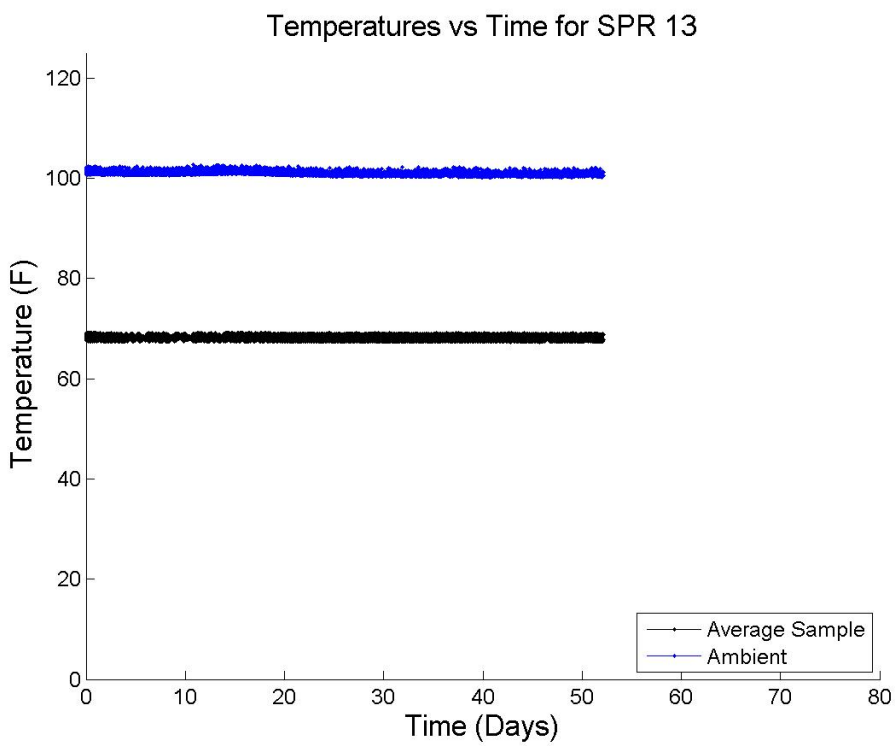

Figure A3-5d. Creep test #13. Plot of temperature versus time. Confining pressure = 1100 psi, Stress difference = 3250 psi and Temperature = 100°F. Recovery Depth = 1089 ft.

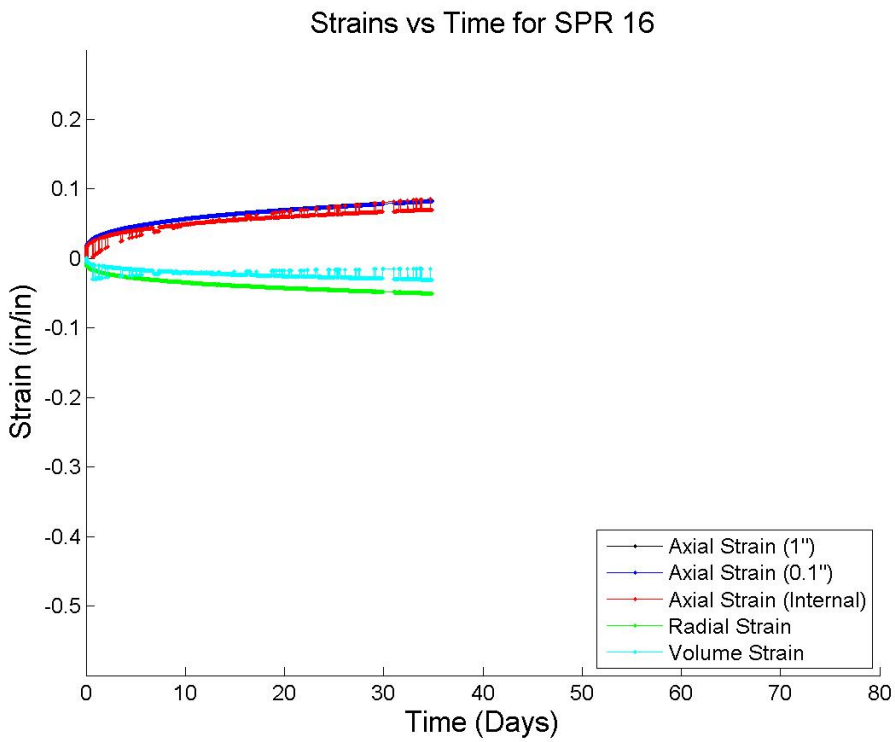

Figure A3-6a. Creep test #16. Plot of all strains versus time. Confining pressure = 1100 psi, Stress difference = 3750 psi and Temperature = 100°F. Recovery Depth = 1092.5 ft.

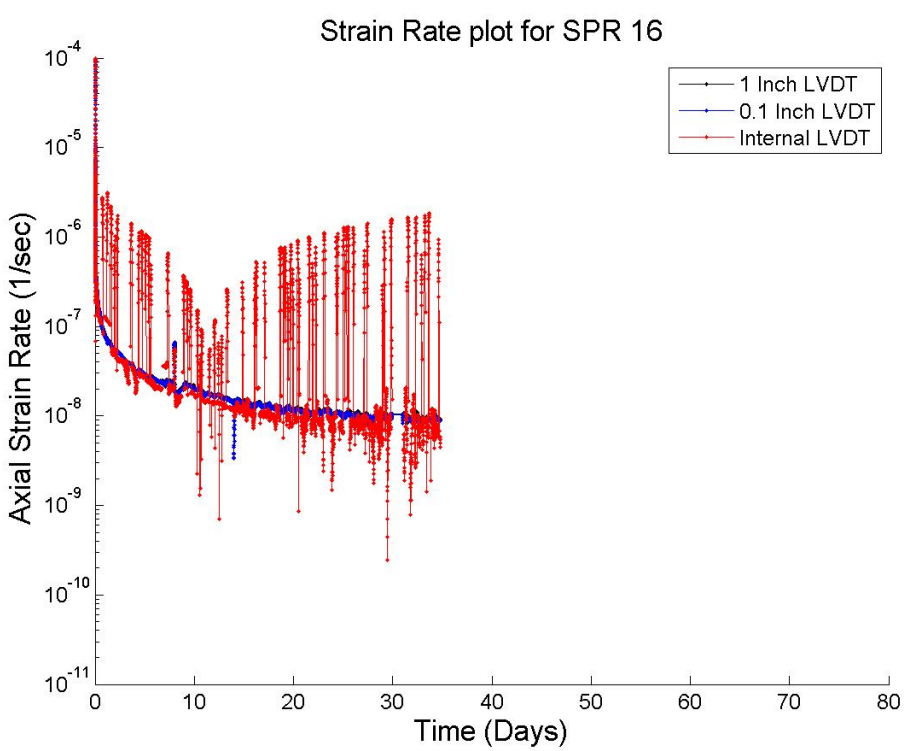

Figure A3-6b. Creep test #16. Plot of strain rates versus time. Confining pressure = 1100 psi, Stress difference = 3750 psi and Temperature = 100°F. Recovery Depth = 1092.5 ft.

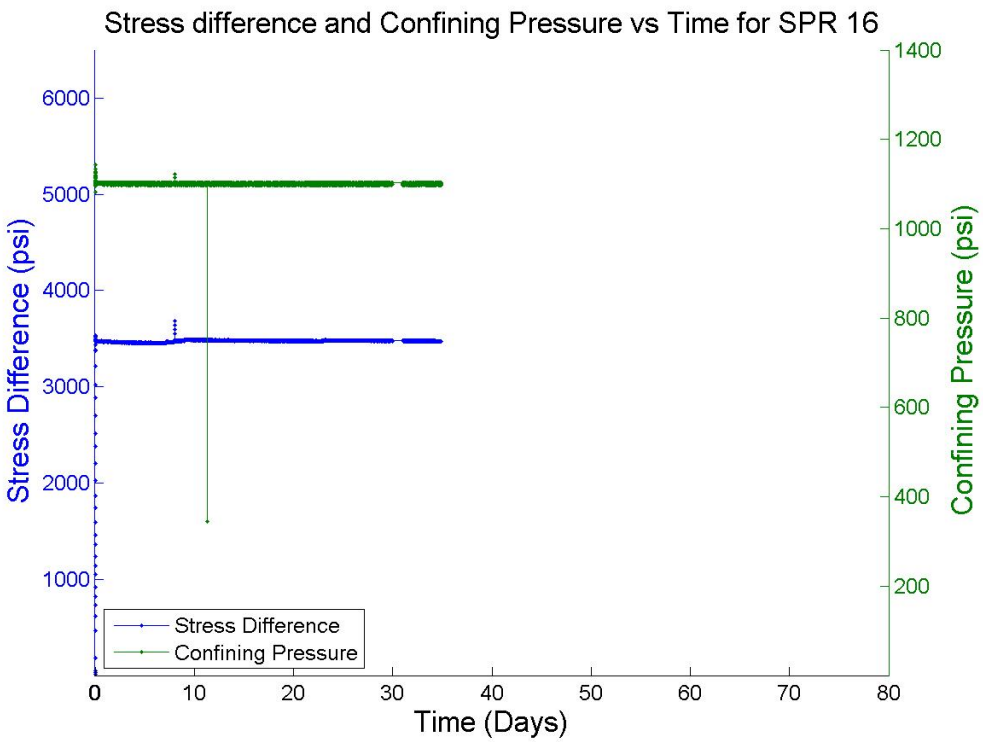

Figure A3-6c. Creep test #16. Plot of stress versus time. Confining pressure = 1100 psi, Stress difference = 3750 psi and Temperature = 100°F. Recovery Depth = 1092.5 ft.

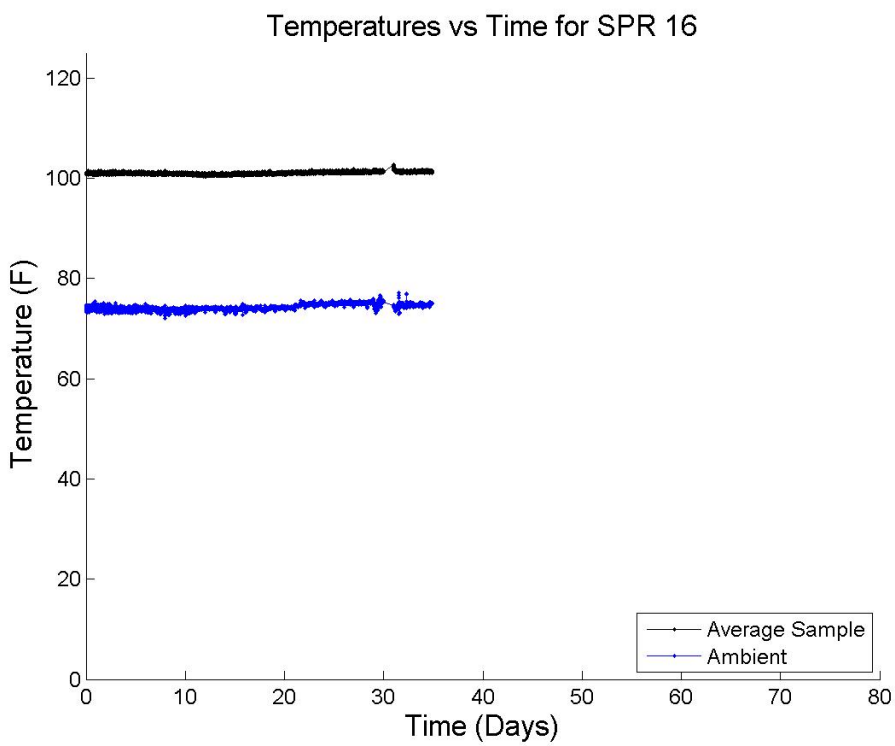

Figure A3-6d. Creep test #16. Plot of temperature versus time. Confining pressure = 1100 psi, Stress difference = 3750 psi and Temperature = 100°F. Recovery Depth = 1092.5 ft.

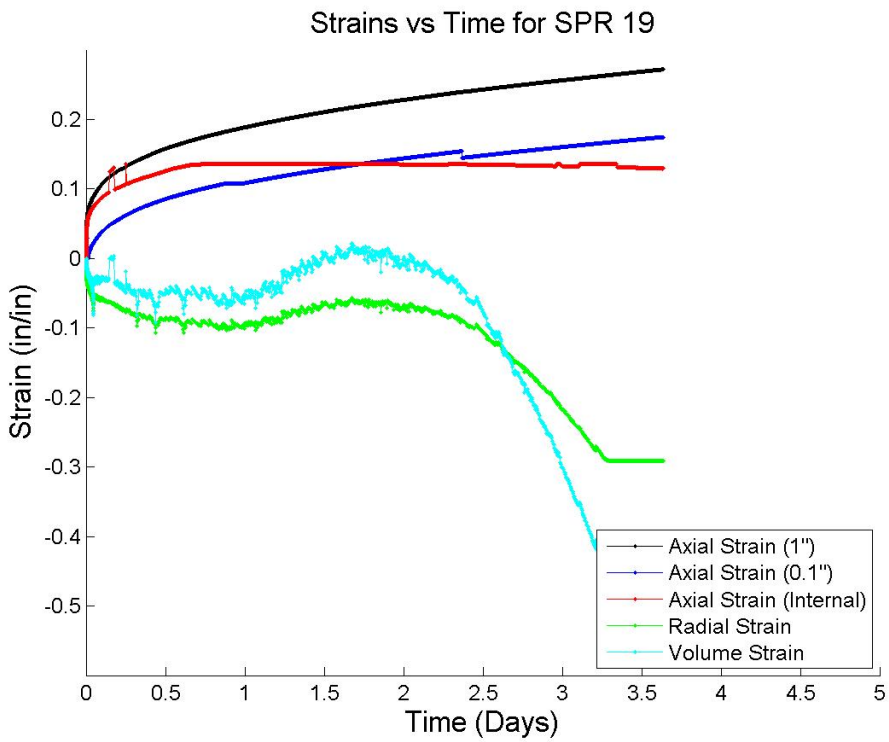

Figure A3-7a. Creep test #19. Plot of all strains versus time. Confining pressure = 1100 psi, Stress difference = 5850 psi and Temperature = 100°F. Recovery Depth = 1095.9 ft. Due to the high strains in achieved on this specimen, the internal LVDTs and radial Schuler gage both ran out of range. Note: This graph is plotted on a different scale.

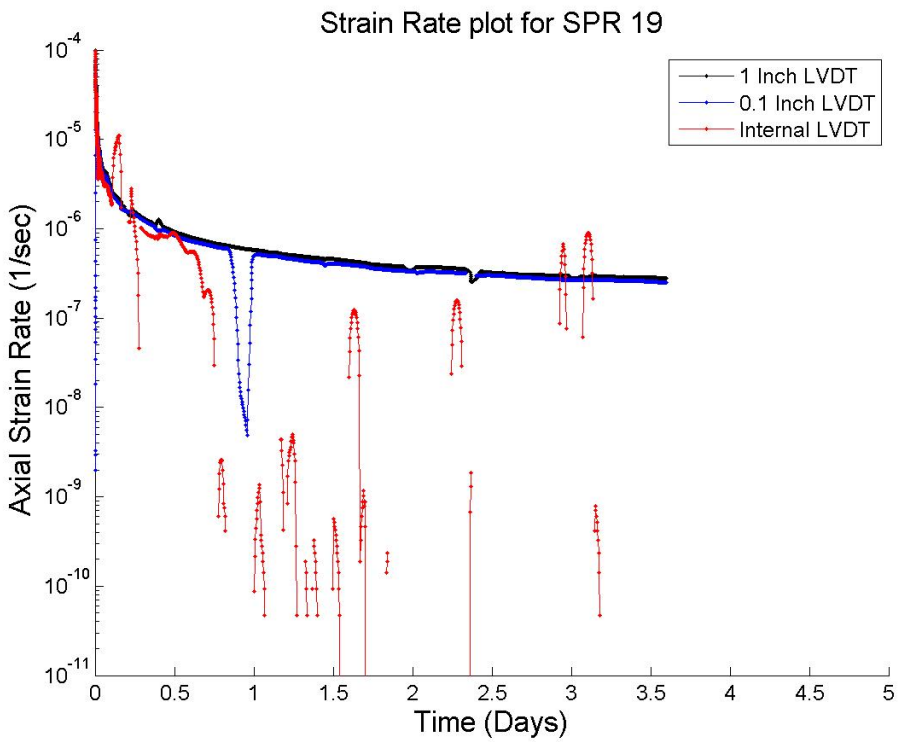

Figure A3-7b. Creep test #19. Plot of strain rates versus time. Confining pressure = 1100 psi, Stress difference = 5850 psi and Temperature = 100°F. Recovery Depth = 1095.9 ft. Due to the high strains in achieved on this specimen, the internal LVDTs and radial Schuler gage both ran out of range. Note: This graph is plotted on a different scale.

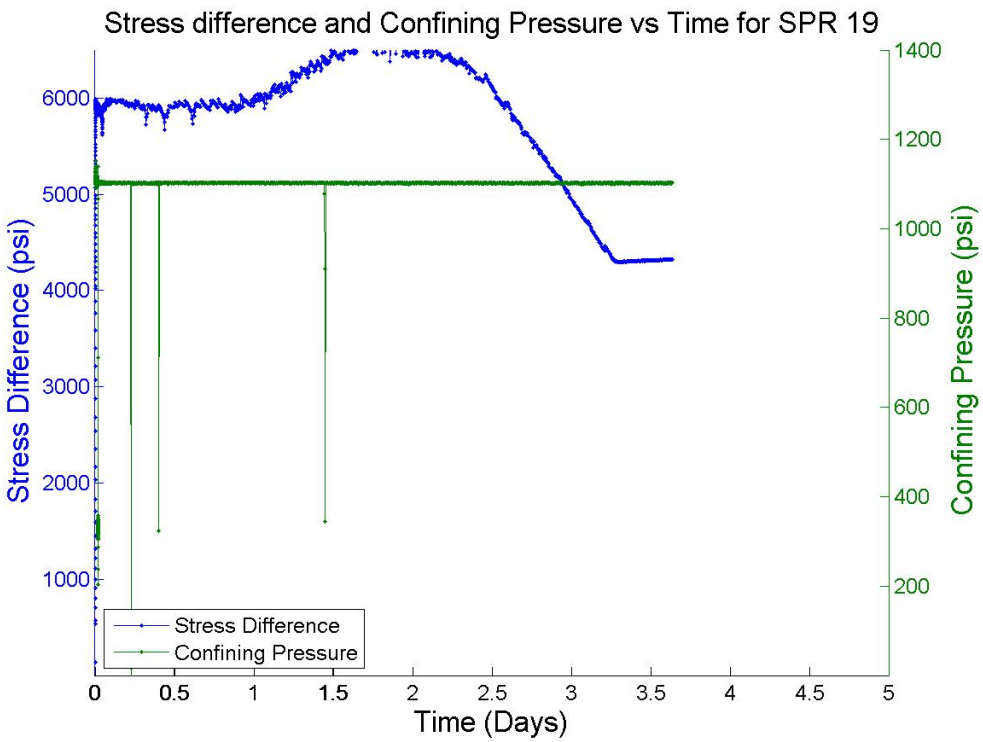

Figure A3-7c. Creep test #19. Plot of stress versus time. Confining pressure = 1100 psi, Stress difference = 5850 psi and Temperature = 100°F. Recovery Depth = 1095.9 ft. Note: This graph is plotted on a different scale.

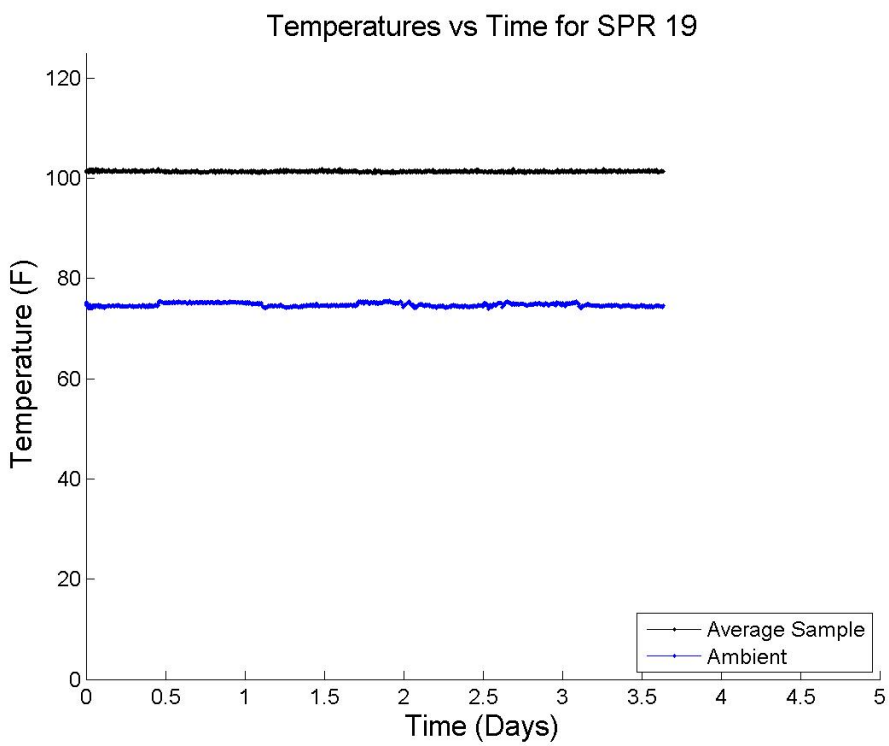

Figure A3-7d. Creep test #19. Plot of temperature versus time. Confining pressure = 1100 psi, Stress difference = 5850 psi and Temperature = 100°F. Recovery Depth = 1095.9 ft. Note: This graph is plotted on a different scale.

DISTRIBUTION:
U.S. Department of Energy (electronic copy only)
Strategic Petroleum Reserve Project Management Office
900 Commerce Road East
New Orleans, LA 70123

U.S. Department of Energy (3)
Strategic Petroleum Reserve Program Office
1000 Independence Avenue, SW
Washington, DC 20585
ATTN: D. Johnson, FE-40

Sandia Internal:

MS 0706 D.J. Borns, 6912 (electronic copy)
MS 0735 E. Webb, 6910 (electronic copy)
MS 0735 M.Y Lee, 6914 (electronic copy)
MS 0735 M.D. Ingraham, 6914 (electronic copy)
MS 0751 B.Y. Park, 6914 (electronic copy)
MS 0751 T.A. Dewers, 6914 (electronic copy)
MS 0899 Technical Library, 9536 (electronic copy)
MS 1031 S.T. Broome, 6914 (electronic copy)
MS 1031 G.M. Flint, 6914 (electronic copy)
MS 1031 P.C. Barrow, 6914 (electronic copy)
MS 1033 S.J. Bauer, 6914 (electronic copy)
MS 9018 Central Tech. Files, 8944 (electronic copy)

Sandia National Laboratories